Available online at www.sciencedirect.com

SCIENCE DIRECT®

Journal of volcanology and geothermal research

ELSEVIER

Journal of Volcanology and Geothermal Research 150 (2006) 55–78

www.elsevier.com/locate/jvolgeores

# Constraints on the mechanism of long-term, steady subsidence at Medicine Lake volcano, northern California, from GPS, leveling, and InSAR

Michael Poland [a,*], Roland Bürgmann [b,1], Daniel Dzurisin [a,2], Michael Lisowski [a,3], Timothy Masterlark [c,4], Susan Owen [d,5], Jonathan Fink [e,6]

[a] *USGS Cascades Volcano Observatory, 1300 SE Cardinal Ct., Suite 100, Vancouver, WA 98683-9589, United States*
[b] *University of California, Berkeley, Department of Earth and Planetary Science, 301 McCone Hall, Berkeley, CA 94720-4767, United States*
[c] *USGS EROS Data Center, SAIC, Sioux Falls, SD 57198, United States*
[d] *Department of Earth Sciences, University of Southern California, 3651 Trousdale Parkway, Los Angeles, CA 90089, United States*
[e] *Department of Geological Sciences, Box 871404, Arizona State University, Tempe, AZ 85287-1404, United States*

Received 1 June 2004; received in revised form 30 November 2004
Available online 24 August 2005

**Abstract**

Leveling surveys across Medicine Lake volcano (MLV) have documented subsidence that is centered on the summit caldera and decays symmetrically on the flanks of the edifice. Possible mechanisms for this deformation include fluid withdrawal from a subsurface reservoir, cooling/crystallization of subsurface magma, loading by the volcano and dense intrusions, and crustal thinning due to tectonic extension (Dzurisin et al., 1991 [Dzurisin, D., Donnelly-Nolan, J.M., Evans, J.R., Walter, S.R., 1991. Crustal subsidence, seismicity, and structure near Medicine Lake Volcano, California. Journal of Geophysical Research 96, 16, 319-16, 333.]; Dzurisin et al., 2002 [Dzurisin, D., Poland, M.P., Bürgmann, R., 2002. Steady subsidence of Medicine Lake Volcano, Northern California, revealed by repeated leveling surveys. Journal of Geophysical Research 107, 2372, doi:10.1029/2001JB000893.]). InSAR data that approximate vertical displacements are similar to the leveling results; however, vertical deformation data alone are not sufficient to distinguish between source mechanisms. Horizontal displacements from GPS were collected in the Mt. Shasta/MLV region in 1996, 1999, 2000, 2003, and 2004. These results suggest that the region is part of the western Oregon block that is rotating about an Euler pole in eastern Oregon. With this rotation removed, most sites in the

* Corresponding author. Present address: USGS Hawaiian Volcano Observatory, 1 Crater Rim Drive, Hawaii National Park, HI 96718-0051. Tel.: +1 808 967 8891.

*E-mail addresses:* mpoland@usgs.gov (M. Poland), burgmann@seismo.berkeley.edu (R. Bürgmann), dzurisin@usgs.gov (D. Dzurisin), mlisowski@usgs.gov (M. Lisowski), masterlark@geo.ua.edu (T. Masterlark), owen@terra.usc.edu (S. Owen), jon.fink@asu.edu (J. Fink).

[1] Tel.: +1 510 643 9545.
[2] Tel.: +1 360 993 8909.
[3] Tel.: +1 360 993 8933.
[4] Present address: Department of Geological Sciences, University of Alabama, Tuscaloosa, AL 35487, USA. Tel.: +1 205 348 5095.
[5] Tel.: +1 213 740 6308.
[6] Tel.: +1 480 965 5081.

0377-0273/$ - see front matter. Published by Elsevier B.V.
doi:10.1016/j.jvolgeores.2005.07.007

network have negligible velocities except for those near MLV caldera. There, measured horizontal velocities are less than predicted from ~10 km deep point and dislocation sources of volume loss based on the leveling data; therefore volumetric losses simulated by these sources are probably not causing the observed subsidence at MLV. This result demonstrates that elastic models of subsurface volume change can provide misleading results where additional geophysical and geological constraints are unavailable, or if only vertical deformation is known. The deformation source must be capable of causing broad vertical deformation with comparatively smaller horizontal displacements. Thermoelastic contraction of a column of hot rock beneath the volcano cannot reproduce the observed ratio of vertical to horizontal surface displacements. Models that determine deformation due to loading by the volcano and dense intrusions can be made to fit the pattern of vertical displacements by assuming a weak upper crust beneath MLV, though the subsidence rates due to surface loading must be lower than the observed displacements. Tectonic extension is almost certainly occurring based on fault orientations and focal mechanisms, but does not appear to be a major contributor to the observed deformation. We favor a model that includes a combination of sources, including extension and loading of a hot weak crust with thermal contraction of a cooling mass of rock beneath MLV, which are processes that are probably occurring at MLV. Future microgravity surveys and the planned deployment of an array of continuous GPS stations as part of a Plate Boundary Observatory volcano cluster will help to refine this model.
Published by Elsevier B.V.

*Keywords:* GPS; leveling; InSAR; volcano deformation; subsidence; Medicine Lake volcano

## 1. Introduction

Subsidence in volcanic regions is a common yet poorly understood phenomenon that has not been widely studied, perhaps because it is not generally associated with hazardous volcanic processes. For example, deformation of the Phlegrean Fields near Naples, Italy during the last ~2000 yr includes centuries-long periods of subsidence at 1–2 cm/yr (e.g., Yokoyama, 1971). However, little research has attempted to explain this deformation, which has been attributed to self-loading compaction (Yokoyama, 1971), while much work has been published on the episodic uplift of the caldera floor since about 1970. The few subsiding volcanoes that have received attention are sites of recent eruptions, and proposed mechanisms include magma loss due to eruption (Sigmundsson et al., 1992; Dvorak and Dzurisin, 1997), contraction due to cooling and crystallization of magma at depth (Sigmundsson et al., 1997; Sturkell and Sigmundsson, 2000), and magma drainage from a shallow reservoir (De Zeeuw-van Dalfsen et al., 2005). The causes of subsidence at volcanoes that have not erupted recently, including the Phlegrean Fields, have not been examined in detail. Nevertheless, volcano subsidence can be a significant phenomenon at potentially active volcanoes and deserves further consideration.

An excellent location for investigating the subsidence of dormant volcanoes is in northeastern California at Medicine Lake volcano (MLV; Fig. 1). MLV is a late Pleistocene–Holocene shield located on the Modoc Plateau, approximately 50 km east–northeast of Mt. Shasta (Donnelly-Nolan, 1988). Leveling surveys at MLV in 1954, 1989, 1990, and 1999 indicate long-term, steady subsidence maximized in the summit caldera and decaying symmetrically on the flanks of the edifice (Dzurisin et al., 1991, 2002).

The subsidence may be caused by a variety of mechanisms, including fluid withdrawal, cooling or crystallization of magma, loading by the volcano and dense intrusions, crustal thinning due to tectonic extension, or some combination of factors. Dzurisin et al. (1991, 2002) favored a combination of models including crustal thinning due to Basin and Range extension coupled with loading by the volcano and subvolcanic intrusions, both facilitated by heat-induced weakening of the crust. Because vertical deformation data alone cannot distinguish between these possibilities, we conducted multiple GPS campaigns between 1996 and 2004 to obtain horizontal displacements in the MLV–Mt. Shasta region in an attempt to better constrain the source of the deformation.

## 2. Geology of Medicine Lake volcano

MLV is the largest volcano by volume in the Cascade Range, with lavas that cover 2200 $km^2$ and

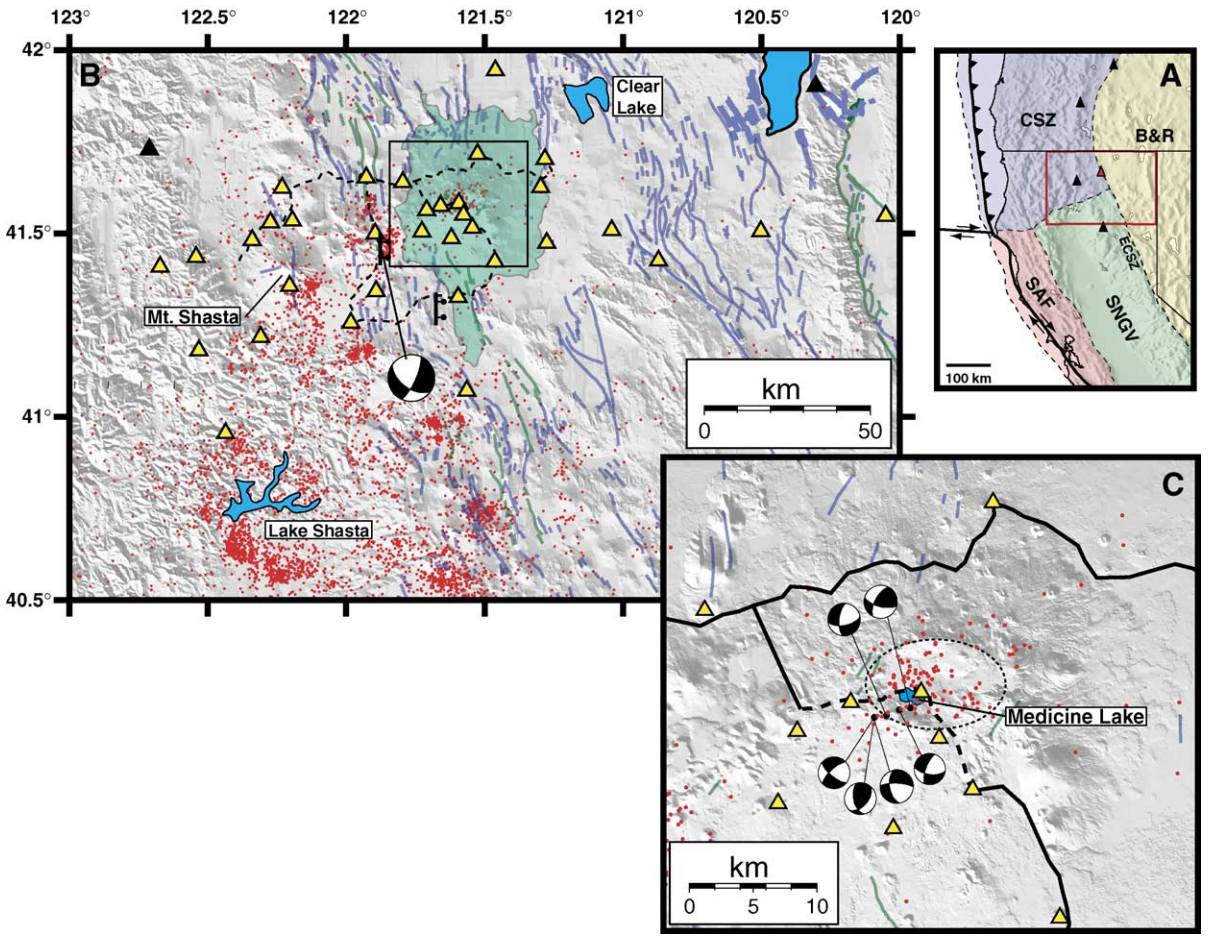


Fig. 1. Maps showing geologic features and geodetic networks in the MLV region. (A) Location map showing general tectonic provinces of northern California and relative motions (modified from Wells et al., 1998) including the San Andreas Fault (SAF, red region), Basin and Range (B & R, yellow region), Cascadia Subduction Zone and volcanic arc (CSZ, purple region), and Sierra Nevada/Great Valley block (SNGV, green region). The Eastern California Shear Zone–Walker Lane belt of dextral shear (ECSZ) separates the B & R from the SNGV block. Volcanoes of the Cascade arc are noted by black triangles. Medicine Lake volcano is noted by the red triangle. Area of part B is shown by the red box. (B) Shaded relief map of northeastern California showing all earthquakes that were recorded through July 2004 (red dots) from the Northern California Earthquake Data Center, Quaternary and Holocene faults (blue and green lines, respectively) from Jennings (1994), campaign GPS stations (yellow triangles), continuous GPS stations (black triangles), and leveling lines (dashed black lines). The approximate aerial extent of lava flows from MLV as reported by Donnelly-Nolan (1988) is shaded light green. Focal mechanism is for the largest event of the 1978 Stephens Pass swarm (Patton and Zandt, 1991). Two historical normal faulting events, inferred from leveling data (Dzurisin et al., 2002), are shown with the bar-and-ball on the downthrown side. Area displayed in part C is within the black-lined box. (C) Shaded relief map showing the summit region of MLV. Symbols are the same as in part B, except that solid black lines are leveling routes, with the dashed black segment showing that portion of the leveling line that was surveyed in 1999. The summit caldera is outlined by a dotted line. Focal mechanisms are from the 1988–1989 earthquake swarm and were obtained from the Northern California Earthquake Data Center.

occupy a volume of 600 $km^3$ (Donnelly-Nolan, 1988). The volcano rises 1200 m above the Modoc Plateau, reaching an elevation of 2376 m, and a $7 \times 12$ km caldera elongate about an east–west axis occupies the summit region (Donnelly-Nolan and Nolan, 1986; Donnelly-Nolan and Ramsey, 2001). The geological characteristics of MLV were first documented by Peacock (1931) and Powers (1932), and the volcano was later mapped and described by Anderson (1941). New mapping and geochemical studies (e.g. Gerlach and

Grove, 1982; Grove et al., 1982; Grove and Donelly, 1986; Donnelly-Nolan, 1988; Grove et al., 1988; Donnelly-Nolan et al., 1990; Donnelly-Nolan et al., 1991) have led to a greater understanding of the volcanic and petrologic history of MLV.

In the past 11,000 yr, 17 eruptions have occurred at MLV with compositions ranging from basalt to rhyolite and amounting to an extruded volume of approximately 7.8 $km^3$ (Donnelly-Nolan et al., 1990). This post-glacial activity has occurred in two episodes, with 8 mafic eruptions occurring within a few hundred years starting about 11,000 ka and 9 additional eruptions with products ranging from basalt to rhyolite after a hiatus of ~6000 yr (Donnelly-Nolan et al., 1990). The most recent eruption occurred ~900 yr ago at Glass Mountain on the eastern edge of the caldera, where about 1 $km^3$ of rhyolite and dacite were erupted from numerous aligned vents, forming a steep sided lava flow and several coalescing domes in addition to an initial rhyolitic tephra fall deposit (Donnelly-Nolan et al., 1990). Vent and ground crack alignments at Glass Mountain and other recent silicic eruption sites have been interpreted as evidence of subsurface feeder dikes (Fink and Pollard, 1983).

Models of the magmatic system at MLV have been proposed by Heiken (1978), Eichelberger (1981), and Donnelly-Nolan (1988). The chemical similarity of silicic lavas on opposite sides of the caldera led Heiken (1978) to infer a common silicic reservoir at depth. Eichelberger (1981) suggested that a large silicic magma chamber, formed due to heating by underplating by mafic magmas, is responsible for the recent rhyolitic eruptions. Finally, Donnelly-Nolan (1988) proposed that the extensional tectonic setting at MLV favors a magmatic system consisting of numerous dikes, sills, and other small intrusive bodies of magma of varying compositions.

Geophysical and geological studies of the volcano suggest the presence of both an aerially extensive solidified intrusive complex of several hundred thousand years in age in addition to recent smaller intrusions. On the basis of gravity studies, Finn and Williams (1982) inferred a dense (0.41 $g/cm^3$ greater than surrounding rocks), cone-shaped body extending from depths of 1.5 to 4 km below MLV caldera with a diameter of 9 km at the top and an elliptically shaped base measuring 20 by 36 km elongate in an east–west direction. Fuis et al. (1987) and Zucca et al. (1986) identified a high-velocity feature at 1–2 km depth under the caldera from seismic refraction data, and Stanley et al. (1990) imaged the same feature as a high-resistivity, high-velocity body using magnetotelluric and refraction data. Seismic tomography of the crust beneath MLV by Ritter and Evans (1997) reveals a high-velocity anomaly in the upper crust (0–10 km depth) under the caldera. Thus, the MLV subsurface apparently includes a shallow, large, cone-shaped solidified intrusion at ~1–4 km depth with a solidified intrusive complex extending to depths of at least 10 km (Fig. 2).

During geothermal exploration in the 1970s and 1980s, two drillholes penetrated a body of granodiorite beneath MLV caldera at depths below about 2.5 km (Lowenstern et al., 2003). U–Pb dating of zircons from this unit indicates emplacement at about 320 ka, followed by alteration (associated with development of a shallow hydrothermal system) prior to about 170 ka (Lowenstern, 1999; Lowenstern et al., 2003). The granodiorite intrusion is at approximately the same depth as the upper-level high-velocity body described above. A typical granodiorite density of 2.7–2.8 $g/cm^3$ is greater by about 0.4 $g/cm^3$ than surrounding rhyolitic rocks (also recovered in drillcore) of the early MLV edifice, which agrees with the gravity results of Finn and Williams (1982). Thus, the 320 ka granodiorite intrusion is apparently the dense, high-velocity, resistive body imaged by geophysical techniques. Unaltered granitoid xenoliths have also been found within some Holocene lavas at MLV (Lowenstern et al., 2000). Dating by U–Th disequilibrium indicates that several of the xenoliths crystallized less than 25,000 yr BP. These unaltered felsic intrusives do not appear in the exploratory drill holes (the deepest of which reached $<3$ km below MLV), suggesting the presence of a variety of small intrusive bodies located at shallow depths (3–6 km) beneath or perhaps within the large, altered, 320 ka granodiorite (Lowenstern et al., 2000, 2003) and supporting the magmatic model of Donnelly-Nolan (1988).

The presence of liquid melt at depth below MLV is proposed by Evans and Zucca (1988) and Chiarabba et al. (1995), who identified a low-velocity, high-attenuation body at 3–5 km depth below the previously recognized cone-shaped high-velocity body under MLV caldera. The low velocity body is prob-

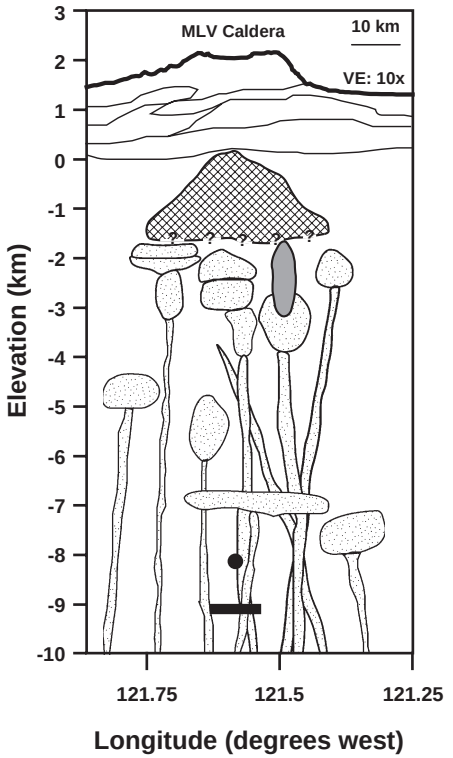


Fig. 2. Schematic E–W cross section model of the MLV subsurface, based in part on that of Donnelly-Nolan (1988). Vertical exaggeration is 10×. Felsic and mafic lava flows of the early MLV shield underlie the caldera (Donnelly-Nolan, 1988). A large, cone-shaped granodiorite intrusion at depths of about 1.5–4 km (cross-hatched pattern) has been identified in drill core and by geophysical investigations (Finn and Williams, 1982; Zucca et al., 1986; Fuis et al., 1987; Lowenstern, 1999; Lowenstern et al., 2003). The only area of possible liquid melt as deduced from seismic data (Evans and Zucca, 1988; Chiarabba et al., 1995) occurs at 4–6 km beneath the eastern caldera rim (gray shaded area), which was the site of the most recent volcanic eruption. An extensive complex of solidified mafic and felsic intrusive bodies (dotted pattern) is inferred beneath the granodiorite intrusion to below 10 km depth (Evans and Zucca, 1988; Lowenstern et al., 2003). The best-fitting point and dislocation sources of volume loss to leveling data determined by Dzurisin et al. (2002) are shown as a black circle and rectangle, respectively. Note that both sources are significantly below the modeled location of magma based on interpretation of seismic data (Evans and Zucca, 1988; Chiarabba et al., 1995).

ably a small (~10 km$^3$) zone of silicic magma, which is the only zone of melt recognized beneath MLV. One long-period earthquake was recorded at 15 km depth in December 1989 (Pitt et al., 2002), and may be additional evidence of liquid magma within the crust (Dzurisin et al., 1991).

## 3. Tectonic setting and recent seismicity

MLV is located east of the axis of the Cascade volcanic arc (formed as a result of the Cascadia subduction zone) and on the western margin of the Basin and Range extensional province, which is defined by the Eastern California Shear Zone (ECSZ)–Walker Lane belt of dextral shear (Fig. 1A). Deformation and seismicity in the MLV region are a consequence of the interactions between the different tectonic regimes, in addition to local volcanic sources.

### *3.1. Basin and Range/Eastern California Shear Zone*

Geodetic studies indicate that deformation in the Basin and Range province is characterized by east–west extension at the eastern margin of the province transitioning to right lateral shear in the west (Dixon et al., 1995; Thatcher et al., 1999; Dixon et al., 2000; Bennett et al., 2003). Clear evidence for Basin and Range tectonism at MLV is manifested as normal faults, which are located both north and south of the volcano and presumably exist under the volcanic pile (Fig. 1B) (Donnelly-Nolan, 1988; Jennings, 1994; Blakely et al., 1997). Blakely et al. (1997) noted that the fault geometry varies from N–S in the northern part of the MLV/Mt. Shasta region to NW–SE south of the volcanoes, and attributes the change in fault orientation to the interaction between the Walker Lane to the south and Cascade arc to the north. One such kink occurs in a fault located directly beneath MLV caldera.

Three episodes of seismicity have been documented in the MLV region. The first took place in 1978 near Stephens Pass, located between MLV and Mt. Shasta. All earthquakes were shallow and occurred on a north-trending fault zone with an eastward dip, similar to other normal faults in the region. Vertical offsets measured along the fault zone were 1–1.5 m (Bennett et al., 1979). A focal mechanism recorded during the largest event of the swarm ($M_L$=4.6 on August 1, 1978; Patton and Zandt, 1991) indicates normal motion with a component of right-lateral slip (Fig. 1B). Dzurisin et al. (2002) modeled 0.90 ± 0.02 m of normal motion between 2 km depth and the surface based on leveling data that spanned the swarm. Another episode of shallow events was

recorded 10 km north of Stephens Pass in 1981 near the town of Tennant, again along a north-trending fault, though neither ground breakage nor vertical deformation was observed (Dzurisin et al., 1991). In September 1988 through 1989, a swarm of low magnitude, short period, and shallow (<4 km) seismicity occurred under MLV caldera (Walter and Dzurisin, 1989; Dzurisin et al., 1991). The cause of the activity is unclear, and six focal mechanisms from the swarm suggest mostly strike-slip motion with both normal and reverse components (Fig. 1C). The complexity may be related to the change in fault orientation beneath the volcano noted above. An additional faulting event approximately 30 km south of MLV caldera is inferred from the 1954–1989 leveling data collected by Dzurisin et al. (1991, 2002). Their model predicts $0.41 \pm 0.02$ m of slip on an E-dipping normal fault in a region of abundant mapped faults (Fig. 1B). There is no record of significant seismic activity in the region prior to the 1978 earthquakes, however seismic stations were sparse in the region before ~1980 and faulting episodes could have gone undetected (Dzurisin et al., 1991, 2002). Two long-period earthquakes have been detected beneath MLV, on October 14, 1996 (depth uncertain) and December 1, 1989 (depth = 15 km), and may reflect fluid migration at depth (Pitt et al., 2002).

In addition to extension, right-lateral displacement may be occurring in the MLV region due to NW translation of the coherent Sierra Nevada/Great Valley (SNGV) block at approximately 12 mm/yr relative to stable North America (Argus and Gordon, 1991; Sauber et al., 1994; Wells et al., 1998; Thatcher et al., 1999; Dixon et al., 2000; Miller et al., 2001a; Bennett et al., 2003). The Eastern California Shear Zone (ECSZ), along the eastern margin of the SNGV, accommodates much of this displacement and may account for as much as 29% of Pacific–North America plate motion (Dokka and Travis, 1990a; Dokka and Travis, 1990b; Miller et al., 2001a). Dixon et al. (2000) used GPS measurements to infer right-lateral displacement of 6–8 mm/yr at 40° latitude distributed on the Honey Lake and Mohawk Valley fault zones, which agrees with estimates obtained by Thatcher et al. (1999) for the region. Work by Hammond and Thatcher (2003) from a GPS transect immediately south of MLV suggests that a small amount of right-lateral shear is occurring near the latitude of MLV as well. This result is consistent with the presence of several NW-trending dextral fault zones in northeast California and southern Oregon, east of MLV (Pease, 1969; Wright, 1976; Roberts, 1984; Page et al., 1993; Pezzopane and Weldon, 1993), and focal mechanisms from on and around the volcano that suggest strike slip motion (Fig. 1). Consequently, dextral shear associated with the ECSZ probably extends into the MLV region.

### 3.2. Cascadia subduction zone

A second possible source of tectonic deformation in the MLV region is the Cascadia subduction zone, where locking of the main thrust fault at shallow depths results in elastic contraction along an east–west axis (McCaffrey et al., 2000; Murray and Lisowski, 2000; Savage et al., 2000). Deformation due to plate locking is measurable up to 150 km inland in the Cascadia forearc (Savage et al., 2000). For comparison, the westernmost station in the MLV GPS network is ~200 km from the deformation front. Miller et al. (2001b) noted that no residual velocity from strain associated with the subduction zone is detected at a GPS station ~80 km west of MLV; therefore, deformation due to locking of the subduction megathrust is probably not significant within the MLV GPS network. Slow earthquakes have been inferred from the time series of the continuous GPS site YBHB (Fig. 1B), however none of the campaign GPS measurements at MLV occurred during a known transient and the deformation due to these events is on the order of 4 mm (Szeliga et al., 2004). As a result, slow earthquakes do not appear to influence to the overall deformation field around MLV.

A component of arc-parallel displacement is superimposed on the contraction throughout Oregon, indicating rotation of the Cascadia forearc (Wells et al., 1998; McCaffrey et al., 2000; Savage et al., 2000). Wells et al. (1998) proposed that coastal Oregon is rotating clockwise about a vertical axis relative to stable North America due to impingement of the northwest translating SNGV against southern Oregon. Both Blakeley et al. (1997) and McCaffrey et al. (2000) suggested that Oregon block rotation might extend into northern California, which includes the MLV area.

## 4. Leveling data and results

Dzurisin et al. (1991) presented results from a 193 km-long leveling circuit that crosses the summit and flanks of MLV and was measured in 1954 and 1989 (Fig. 1B). They reported a maximum of $11.1 \pm 1.2$ mm/yr of subsidence at the summit of the edifice, which decays rapidly and symmetrically on the flanks. The subsidence rate was later amended by Dzurisin et al. (2002) to $8.6 \pm 0.9$ mm/yr to account for previously unrecognized artifacts in the data. Additional leveling data includes a traverse across the northern flank of MLV that was surveyed in 1954 and 1990 (Fig. 1B), and the 1999 reoccupation of a 25 km segment of the 193 km circuit that crosses MLV caldera (Fig. 1C). Maximum subsidence on the northern traverse is $3.9 \pm 1.0$ mm/yr located 10 km immediately north of MLV caldera (Dzurisin et al., 2002). The purpose of the 1999 survey was to determine whether or not the 1954–1989 subsidence had continued during 1989–1999. The vertical velocity profiles for the two time periods are identical within measurement error, suggesting that the subsidence has been essentially constant in space and time for nearly 50 yr (Dzurisin et al., 2002).

Dzurisin et al. (2002) modeled the leveling results by inverting the data for either a point source of volume loss or a closing mode-dislocation with no dip (approximating a deflating sill) at depth. The point source was located at 10 km depth beneath MLV caldera and had a volume loss of $0.0031 \pm 0.0001$ $km^3$/yr. The sill was also located beneath MLV caldera but was slightly deeper (11 km) with a volume decrease of $0.0020 \pm 0.0001$ $km^3$/yr. Both models predict similar vertical displacements, but different horizontal deformation. Thus, GPS measurements may be able to distinguish between these and other models, and assess the validity of the volume loss mechanism.

## 5. GPS data and results

In September 1996, 24 sites in a broad area of northern California that includes MLV and Mt. Shasta were surveyed using campaign GPS. All stations were occupied for at least 8 h on each of three consecutive days using Trimble 4000 SSE and SSi receivers. The network included 18 sites that had originally been established in 1990 by the USGS Cascades Volcano Observatory (Dzurisin et al., 1991; Yamashita and Wieprecht, 1995). Unfortunately, the 1990 data quality was poor due to the lack of precise orbital tracking, poor satellite constellation, and short occupation times; therefore, those results are not included in this analysis.

The same equipment and techniques used in 1996 were employed for a survey of 35 benchmarks in August 1999. In September 2000, eight sites in the Mt. Shasta region were occupied using Ashtech Z-XII receivers for at least 8 h on each of two consecutive days. An additional 12 sites on and east of MLV were surveyed in June/July 2003 using Trimble 5700, 4700, 4000 SSi, and Ashtech Z-XII receivers for at least 8 h on each of two days (not necessarily consecutive). Finally, a survey of 27 sites was completed in June/July 2004 following the same strategy and using the same equipment as in the previous year. A summary of GPS sites, years occupied, and velocities is given in Table 1. In addition to campaign data, results from the Bay Area Regional Deformation network continuous sites YBHB and MODB (black triangles in Fig. 1B) were included in the analysis.

Daily GPS solutions were determined with the GIPSY/OASIS II software using the point-positioning method (Zumberge et al., 1997) and following the procedures outlined in Savage et al. (2000) and Hammond and Thatcher (2004). Velocities presented in Table 1 and Fig. 3 are with respect to stable North America as defined by Hammond and Thatcher (2004). Uncertainty in the vertical component of deformation is similar to the measured velocities for most stations; therefore, the vertical data are not used in the present analysis. However, it is noteworthy that measured subsidence at site ML02, the only GPS station located in MLV caldera, is $11.9 \pm 3.2$ mm/yr, which resembles the subsidence rate of $8.6 \pm 0.9$ mm/yr determined from leveling surveys.

Deformation across the MLV/Mt. Shasta region relative to stable North America is dominated by a NW velocity component that is probably related to block rotation of western Oregon (Fig. 3). To correct for this motion we used the velocities and uncertain-

Table 1
Locations, occupation histories, and velocities of GPS stations in northeastern California

| Station name[a] | Map ID | Occupation years | | | | | Days[b] | Lat. (°N) | Long. (°E) | Velocities and error (mm/yr)[c] | | | | | | |
|---|---|---|---|---|---|---|---|---|---|---|---|---|---|---|---|---|
| | | 1996 | 1999 | 2000 | 2003 | 2004 | | | | N vel. | E vel. | N σ | E σ | Correl. | U vel. | U σ |
| 047M | 047M | | X | | | X | 5 | 41.5170 | −121.5450 | 6.73 | −5.96 | 1.21 | 1.20 | −0.18 | −1.96 | 4.36 |
| Black Fox | BLKF | X | X | | | X | 9 | 41.3464 | −121.8914 | 3.21 | −7.29 | 0.72 | 0.71 | 0.00 | −0.46 | 2.44 |
| Bullseye Lake | BEYE | X | X | | | X | 7 | 41.5534 | −121.5755 | 6.70 | −6.42 | 0.97 | 0.88 | −0.09 | −4.88 | 3.25 |
| CVO9070 | 9070 | X | X | | | X | 9 | 41.4397 | −122.5412 | 5.56 | −4.87 | 0.73 | 0.72 | −0.02 | 0.39 | 2.45 |
| CVO 9080 | 9080 | X | X | X | | X | 9 | 41.4857 | −122.3397 | 3.56 | −6.70 | 0.81 | 0.78 | 0.01 | −4.46 | 2.72 |
| CVO 9090[d] | 9090 | X | X | | | | 7 | 41.5031 | −121.8939 | 3.72 | −5.50 | 1.25 | 1.21 | 0.06 | −0.06 | 5.12 |
| CVO ML02 | ML02 | X | X | | | X | 7 | 41.5857 | −121.5920 | 3.71 | −4.89 | 0.92 | 0.84 | 0.07 | −11.94 | 3.28 |
| Doe Peak | DOEP | X | X | | X | X | 12 | 41.5077 | −121.7259 | 5.23 | −4.49 | 0.73 | 0.72 | 0.00 | −4.24 | 2.46 |
| Gazelle | GAZE | X | | | | X | 6 | 41.4130 | −122.6729 | 6.07 | −4.93 | 0.74 | 0.73 | −0.01 | −2.96 | 2.52 |
| Herd Peak | HERD | X | X | X | | X | 10 | 41.6282 | −122.2315 | 5.61 | −4.61 | 0.74 | 0.73 | 0.00 | −0.57 | 2.53 |
| Hollenbeck | HLNB | X | X | | X | X | 13 | 41.4779 | −121.2742 | 3.27 | −5.32 | 0.74 | 0.73 | 0.00 | −5.85 | 2.54 |
| HPGN 0204 | 0204 | | X | | | X | 5 | 41.9458 | −121.4615 | 5.52 | −3.17 | 1.06 | 0.99 | −0.04 | −4.34 | 3.77 |
| HPGN 0208 | 0208 | X | X | X | | X | 4 | 41.5321 | −122.2750 | 2.46 | −6.17 | 0.92 | 0.88 | −0.05 | 10.04 | 3.18 |
| HPGN 0210 | CNBY | | X | | X | | 7 | 41.4302 | −120.8706 | 6.02 | −4.23 | 1.14 | 1.09 | −0.04 | 3.18 | 3.86 |
| HPGN 0211 | ALKA | | X | | X | | 6 | 41.5515 | −120.0189 | 3.86 | −3.71 | 1.21 | 1.11 | −0.08 | 18.37 | 3.85 |
| HPGN 0212 | H212 | X | X | | | | 7 | 40.9571 | −122.4349 | 1.87 | −5.39 | 2.24 | 1.98 | −0.13 | 32.20 | 7.03 |
| HPGN 02SS | 02SS | | X | | X | | 5 | 41.5118 | −121.0393 | 4.58 | −4.99 | 1.21 | 1.09 | −0.09 | 11.05 | 4.11 |
| HPGN CA93 | ALTU | | X | | X | | 7 | 41.5097 | −120.5006 | 4.46 | −4.43 | 1.20 | 1.13 | −0.08 | 9.22 | 3.97 |
| Jot Dean | JOTD | X | X | | | X | 7 | 41.4899 | −121.6182 | 6.12 | −4.66 | 0.88 | 0.83 | −0.05 | −6.06 | 2.94 |
| Little Mt. Hoffman | HOFF | | X | | | X | 4 | 41.5788 | −121.6584 | 3.38 | −4.26 | 1.05 | 0.98 | −0.02 | −1.13 | 3.85 |
| M504 | M504 | X | X | | X | X | 10 | 41.7204 | −121.5258 | 4.33 | −5.61 | 0.79 | 0.76 | −0.02 | −2.05 | 2.66 |
| Military Pass | MTRY | | | X | | X | 5 | 41.5340 | −122.1928 | 5.42 | −5.65 | 1.00 | 0.96 | −0.01 | −0.14 | 3.81 |
| Mt. Bradley | BRAD | X | X | X | | X | 13 | 41.2219 | −122.3089 | 4.79 | −6.04 | 0.73 | 0.72 | −0.01 | −3.30 | 2.45 |
| Mumbo | MUMB | X | X | X | | X | 11 | 41.1844 | −122.5326 | 5.01 | −6.06 | 0.74 | 0.73 | −0.01 | −2.24 | 2.50 |
| Overpass | OVRP | X | X | | X | X | 10 | 41.7050 | −121.2814 | 3.78 | −6.47 | 0.77 | 0.76 | 0.02 | −5.89 | 2.61 |
| P501 | P501 | X | X | | | X | 6 | 41.6567 | −121.9284 | 3.64 | −4.27 | 0.79 | 0.77 | 0.00 | −6.03 | 2.65 |
| Pilgrim | PILG | X | X | X | | X | 9 | 41.2597 | −121.9819 | 3.34 | −7.85 | 0.85 | 0.82 | −0.04 | 6.08 | 2.87 |
| Pumice Stone Well | PSWL | | X | | X | X | 9 | 41.5688 | −121.7087 | 5.59 | −2.23 | 0.88 | 0.86 | −0.01 | −1.10 | 3.28 |
| R500 | R500 | X | X | | | X | 6 | 41.3308 | −121.6059 | 3.31 | −6.00 | 0.81 | 0.77 | 0.01 | 1.03 | 2.72 |
| Round Mountain | ROUN | X | X | | X | X | 13 | 41.4273 | −121.4624 | 4.07 | −5.72 | 0.73 | 0.72 | 0.00 | −3.32 | 2.50 |
| Shasta (reset) | SHAS | X | X | X | | X | 8 | 41.3611 | −122.2032 | 3.00 | −7.03 | 0.92 | 0.91 | −0.04 | −1.54 | 3.16 |
| Soldier Mountain | SOLD | | X | | X | | 6 | 41.0742 | −121.5630 | −1.67 | −4.83 | 1.13 | 1.16 | 0.21 | 3.27 | 4.24 |
| Timber Mountain | TMBR | X | X | | X | X | 17 | 41.6292 | −121.2959 | 5.81 | −4.45 | 0.71 | 0.70 | −0.01 | −3.69 | 2.39 |
| Van Bremmer | VANB | X | X | | | X | 7 | 41.6434 | −1121.7947 | 4.08 | −4.08 | 0.76 | 0.74 | 0.00 | −5.74 | 2.57 |
| Modoc Plateau | MODB | continuous, started on November 11, 1999 | | | | | | 41.9023 | −1120.3028 | 0.89 | −3.69 | 1.69 | 1.61 | 0.01 | −5.78 | 7.29 |
| Yreka | YBHB | continuous, started on October 24, 1996 | | | | | | 41.7317 | −1122.7107 | 6.76 | 12.69 | 0.77 | 0.77 | −0.01 | −0.96 | 2.81 |

[a] Only sites with multiple years of data collection are shown.
[b] Total number of days of data collected.
[c] Velocities are in a fixed North America ITRF2000 reference frame.
[d] Site CVO 9090 was destroyed between the 1999 and 2004 surveys.

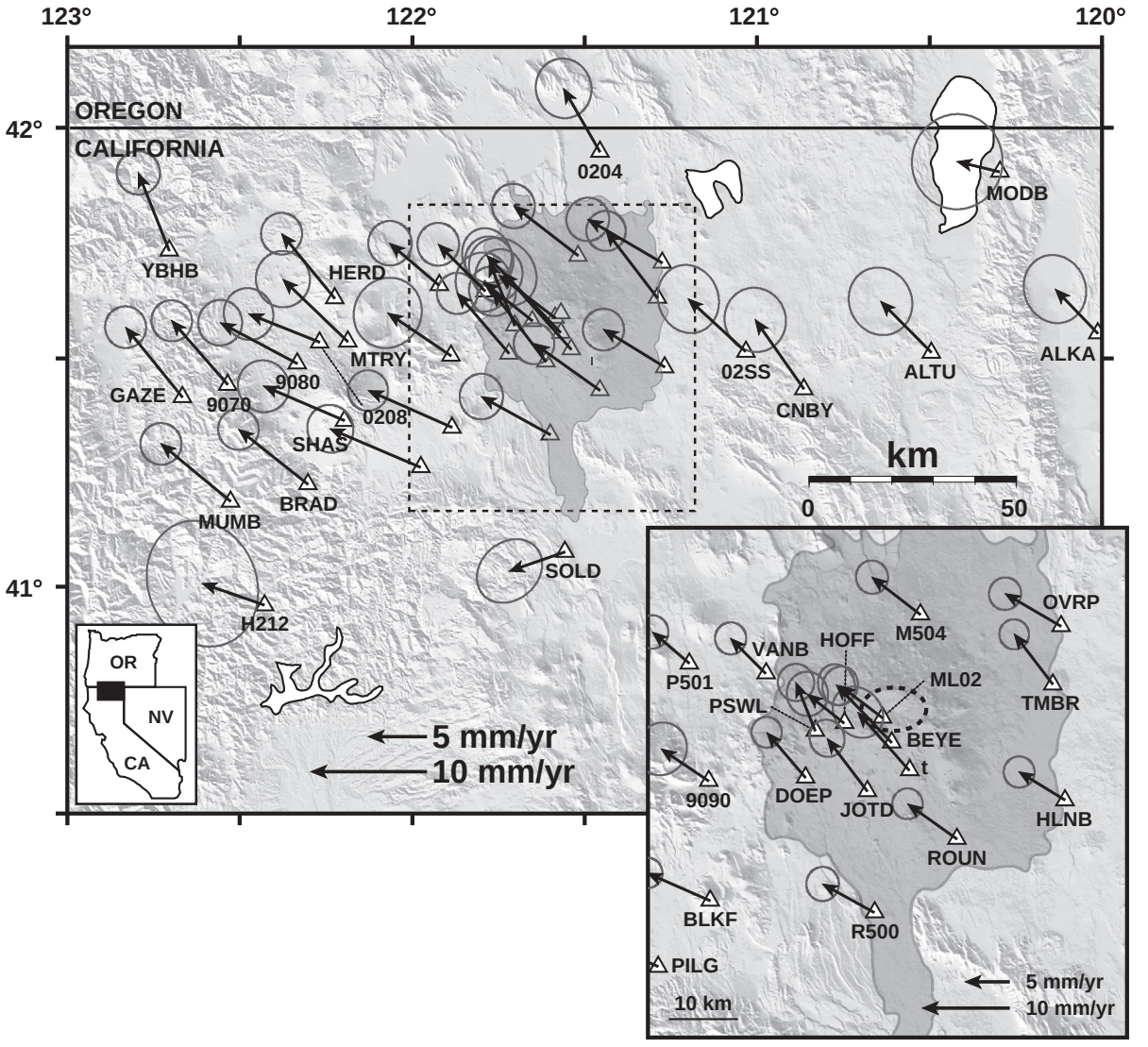


Fig. 3. Horizontal velocities and 95% confidence ellipses for campaign GPS stations in the Mt. Shasta/MLV area of northern California relative to stable North America. Gray shaded area is the approximate aerial extent of MLV lava flows (Donnelly-Nolan, 1988). Dashed square shows area of inset. Dotted ellipse in inset marks the outline of MLV caldera. Note the scale difference between the inset and main vector plots.

ties of 34 stations in northeast California to calculate and remove displacements due to a rigid body rotation (Savage et al., 2001). The sites include 14 that were occupied by Hammond and Thatcher (2003) within about 150 km of MLV. Sites ML02, BEYE, HOFF, 047M, PSWL, JOTD, ROUN, VANB, DOEP, and M504 (Fig. 3) were excluded from the calculation as they may include a component of MLV-related deformation (based on modeling by Dzurisin et al., 2002). Sites SHAS and SOLD were also omitted, the former because of its location on the south flank of Mt. Shasta in an area of historical slope instability and the latter because its motion is clearly anomalous (Fig. 3) and may be caused by poor sky visibility at the site due to a nearby fire lookout tower. The best-fitting Euler pole is located at 43.557°N ± 0.708 latitude and 119.355°W ± 0.842 longitude with a clockwise rotation rate of 1.323°/

Ma ± 0.453. This pole and rotation rate compare favorably to those published by Savage et al. (2000) for southwest Oregon, but the pole is considerably south of those determined geodetically by McCaffrey et al. (2000), geologically and paleomagnetically by Wells et al. (1998) and Wells and Simpson (2001), and seismologically by Lewis et al. (2003) based on data from western Oregon and southwest Washington (Table 2). The discrepancy between data from the southern part of the arc versus the entire arc may indicate that Cascadia does not behave as a single rigid rotating block with no internal deformation, as proposed by Hammond and Thatcher (2003). Strain within the network is not significant at the 95% confidence level and is therefore not considered in the present analysis.

Upon removal of the rotation, most sites in the Mt. Shasta/MLV network have no horizontal velocity within their associated uncertainty, including many of those that are near MLV caldera (Fig. 4). Some exceptions occur in the northern part of the network, including YBHB and 0204. Hammond and Thatcher (2003) suggest that the northern part of the network may lie within a separate tectonic domain that includes southern Oregon and has a slightly different pole and rotation rate than the stations to the south. The residual strain after removal of the rotation is small and approximately the same magnitude as the uncertainty, thus we lack sufficient data to rigorously test this hypothesis. Based on these results, we conclude that the Mt. Shasta/MLV region is part of the western Oregon block, which is rotating clockwise around a pole in eastern Oregon. The anomalous velocity of SOLD may reflect local problems with the site as discussed earlier. A SW-directed displacement is indicated in the area of SHAS, PILG, and BLKF, and may represent the motion of a coherent block SE of Mount Shasta. Finally, subsidence of MLV appears to affect a number of sites around the caldera, though displacements at several are below 95% confidence levels.

Table 2
Euler poles and rotation rates for Cascadia–North America motion determined by this study and other sources

| Source | Euler pole | | Rotation rate (clockwise positive) |
|---|---|---|---|
| | Latitude | Longitude | |
| Wells et al. (1998) | 46.9° | 120.0° | 1.17°/Ma |
| Savage et al. (2000) | 43.4 ± 0.1° | 120.0 ± 0.4° | 1.67 ± 0.32°/Ma |
| McCaffery et al. (2000) | 45.9 ± 0.6° | 118.7 ± 0.7° | 1.05 ± 0.16°/Ma |
| Wells and Simpson (2001) | 45.54° | 119.6° | 1.32 ± 0.16°/Ma |
| This study | 43.6 ± 0.7° | 119.4 ± 0.8° | 1.32 ± 0.45°/Ma |

## 6. InSAR data and results

Additional evidence for steady subsidence at MLV is given by synthetic aperture radar interferometry (InSAR). We processed several ERS-1/2 scenes that cover the summit and eastern flank of MLV. Coherence on the volcano was generally only achieved in interferograms spanning less than 1–2 yr, though one pair provided reasonable coherence over a 4-yr span. This is problematic given that the current rate of subsidence (~9 mm/yr) requires ~4 yr to produce a single interferometric fringe (28.3 mm of range change), of the same order as the uncertainty in the data (Hoffmann and Zebker, 2003). We overcame this difficulty by summing the phase change from three temporally consecutive interferograms spanning the time period April 28, 1993 to July 29, 2000. The resulting stack shows at least two discontinuous but concentric fringes around MLV indicating an increase in interferometric phase (Fig. 5A). Because the look angle of the ERS satellites is relatively steep (~22°), displacements derived from ERS interferograms are a good proxy for vertical deformation (Lu et al., 2000b). Thus, we interpret the increase in range centered on MLV as confirmation of subsidence of the volcano.

To determine the line-of-sight deformation rate we converted the interferometric phase to displacement along a radial transect from the summit of MLV and set the minimum range change arbitrarily equal to 0 mm (Fig. 5b). The results indicate a line-of-sight displacement rate of about −10 mm/yr centered on MLV caldera and extending for a distance of ~15 km, comparable to the rate determined by GPS at ML02 as well as the rate and spatial extent of subsidence measured by leveling. Thus, data from InSAR support our assertion that subsidence at MLV is radially symmetric about the caldera region. The

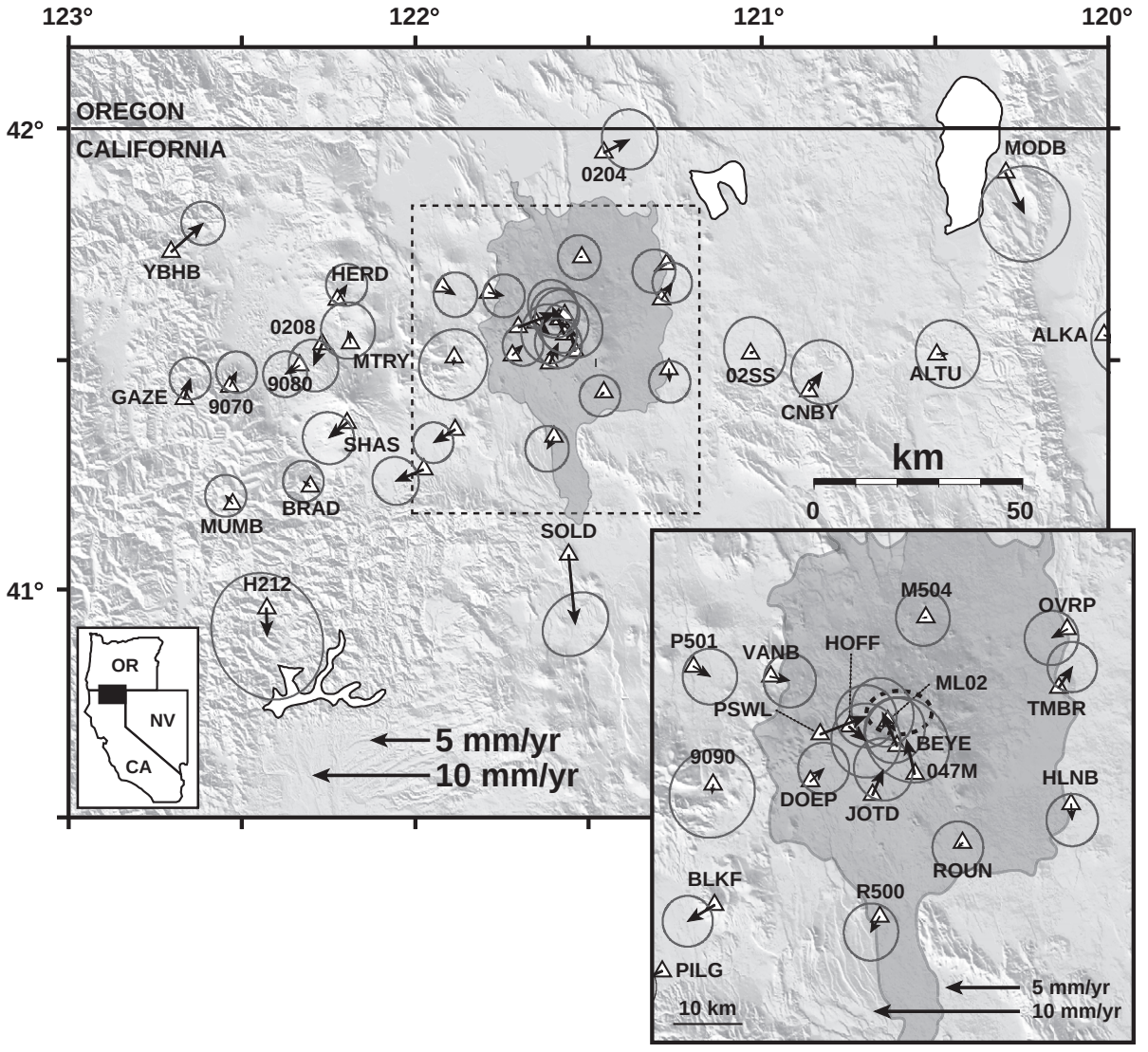


Fig. 4. Horizontal velocities and 95% confidence ellipses after removal of a rigid block rotation about the Euler pole given in Table 2. Symbols are the same as those in Fig. 3. Note the scale difference between the inset and main vector plots.

mechanism that drives this deformation must account for these characteristics.

## 7. Modeling and discussion

The pattern of horizontal displacements determined from GPS measurements is not consistent with a source of volume loss at 10–11 km depth beneath the volcano, as modeled from leveling data (Dzurisin et al., 2002). Both the point and dislocation sources of Dzurisin et al. (2002) predict horizontal displacements radially towards the center of MLV caldera over a broad (~40 km radius) area. However, radial inward deformation is only prevalent at GPS stations that are within about 10 km of the caldera. A simple inverse model of the GPS data using a point source of volume loss (Mogi, 1958) suggests a shallow source (6 km) located almost directly beneath site ML02 (Table 3; Fig. 6A–C).

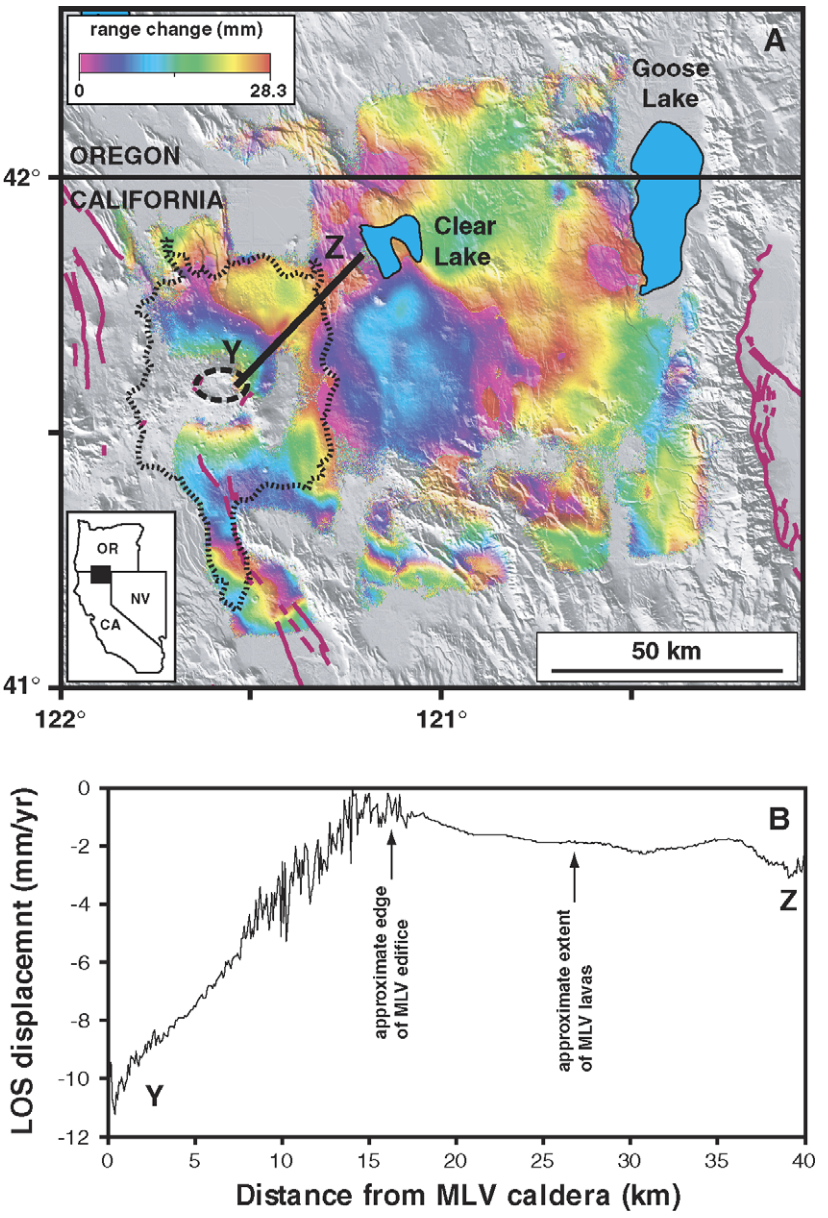


Fig. 5. InSAR data from the MLV region. A) Stack of three interferograms acquired by ERS-1 (orbits 9827 and 21193) and ERS-2 (orbits 22562 and 27572), from track 163, frame 828. The aerial extent of MLV lava flows is noted by a dotted line. MLV caldera is outlined by a dashed line. The total time spanned by the interferogram is 1993–2000. Each full color cycle represents 28.3 mm of line-of-sight range change. Note that although coherence is incomplete, there are approximately 2 color fringes surrounding Medicine Lake volcano that indicate line-of-sight lengthening. B) Profile of line-of-sight displacement in mm/yr along the Y–Z transect shown in part A. Arrows show the approximate extent of the MLV edifice (from topography) and MLV lavas (from Donnelly-Nolan, 1988). Because the ERS satellites have steep look angles (~22°) displacements are approximately vertical. Deformation from InSAR is in good agreement with leveling results, both of which show subsidence maximized within MLV caldera and decaying with radial distance.

Table 3
Modeling results

| Dataset modeled | Source type | Data modeled | Latitude (°N) | Longitude (°W) | Depth (km) | Length (km) | Width (km) | Dip (°) | Strike (°) | Opening (m/yr) | ΔVolume (km³/yr) | WRSS/$(N-P)$[a] |
|---|---|---|---|---|---|---|---|---|---|---|---|---|
| Dzurisin et al. (2002) | Mogi | Leveling | 41.59 | 121.58 | 10 | – | – | – | – | – | −0.0031 ± 0.0001 | 18.31 |
| This study | Mogi | GPS | 41.58 | 121.59 | 6 | – | – | – | – | – | −0.0010 ± 0.0002 | 1.24 |
| Dzurisin et al. (2002) | Sill | Leveling | 41.566–41.637 | 121.559–121.410 | 11 | 10.3 | 4.4 | 0 | 221 | −0.0446 ± 0.0014 | −0.0020 ± 0.0001 | 18.33 |
| This study | Sill | GPS | 41.623–41.616 | 121.499–121.718 | 5 | 18.2 | 9.2 | 0 | 267 | −0.0151 ± 0.0025 | −0.0025 ± 0.0004 | 0.96 |

[a] WRSS/$(N-P)$ is the weighted residual sum of squares normalized by the degrees of freedom and quantified the model misfit. Lower values indicate a better model fit. The values are not directly comparable between Dzurisin et al. (2002) and this study — only between models of the same data type.

The best fitting horizontal dislocation (Okada, 1985), which approximates a deflating sill, is located at a similar depth (5 km) but has a lower misfit than the point source model (Table 3; Fig. 6D–F). Both models are significantly shallower than the best fitting sources modeled from leveling data alone (Table 3), and do a poor job of predicting vertical displacements along the 1954–1989 leveling circuit that crosses the summit of MLV (Fig. 6C and F). To test the depth sensitivity of the dislocation models we calculated the best-fitting horizontal dislocation to each dataset constrained at 0.5 km depth intervals. The resulting depth versus misfit curve (Fig. 7) shows that misfit is minimized at ~11 km for leveling data but is low between about 5 and 15 km. Misfits to GPS data are minimized at 5 km depth and are low between about 4 and 10 km. Although there is some overlap between these regions, the minimal misfits clearly occur at shallower depths for models of GPS data than for leveling (lowest parts of curves in Fig. 7). The simple sources that provided excellent fits to the leveling data (Dzurisin et al., 2002) cannot explain the horizontal velocities measured with GPS. Therefore, the subsidence mechanism at MLV must be able to predict the broad vertical deformation while requiring minimal horizontal displacements.

Another constraint on the mechanism of deformation is the relatively high rate of historical subsidence compared to the deformation history over the life of MLV. Although the leveling data suggest that the subsidence has been occurring at a constant rate for almost 50 yr, this rate cannot have been maintained for a significant portion of the volcano's history. A simple extrapolation of the current rate of 8.6 ± 0.9 mm/yr demonstrates that the total subsidence would be ~8.6 m after 1000 yr, 86 m after 10,000 yr, and 860 m (more than two-thirds of the total height of the volcano) in 100,000 yr (Dzurisin et al., 2002). Evidence from $^{40}Ar/^{39}Ar$ suggests that the volcano has been active for approximately 500,000 yr (J. Donnelly-Nolan, unpublished data). A limitation on the amount of total subsidence at MLV is evident from the distribution of an 180,000 ka silicic tuff (the "dacite tuff of Antelope Well") mapped by Donnelly-Nolan (written communication, 2004). Based on drill core and surface outcrops, she finds that the unit occurs 240–440 m lower in eleva-

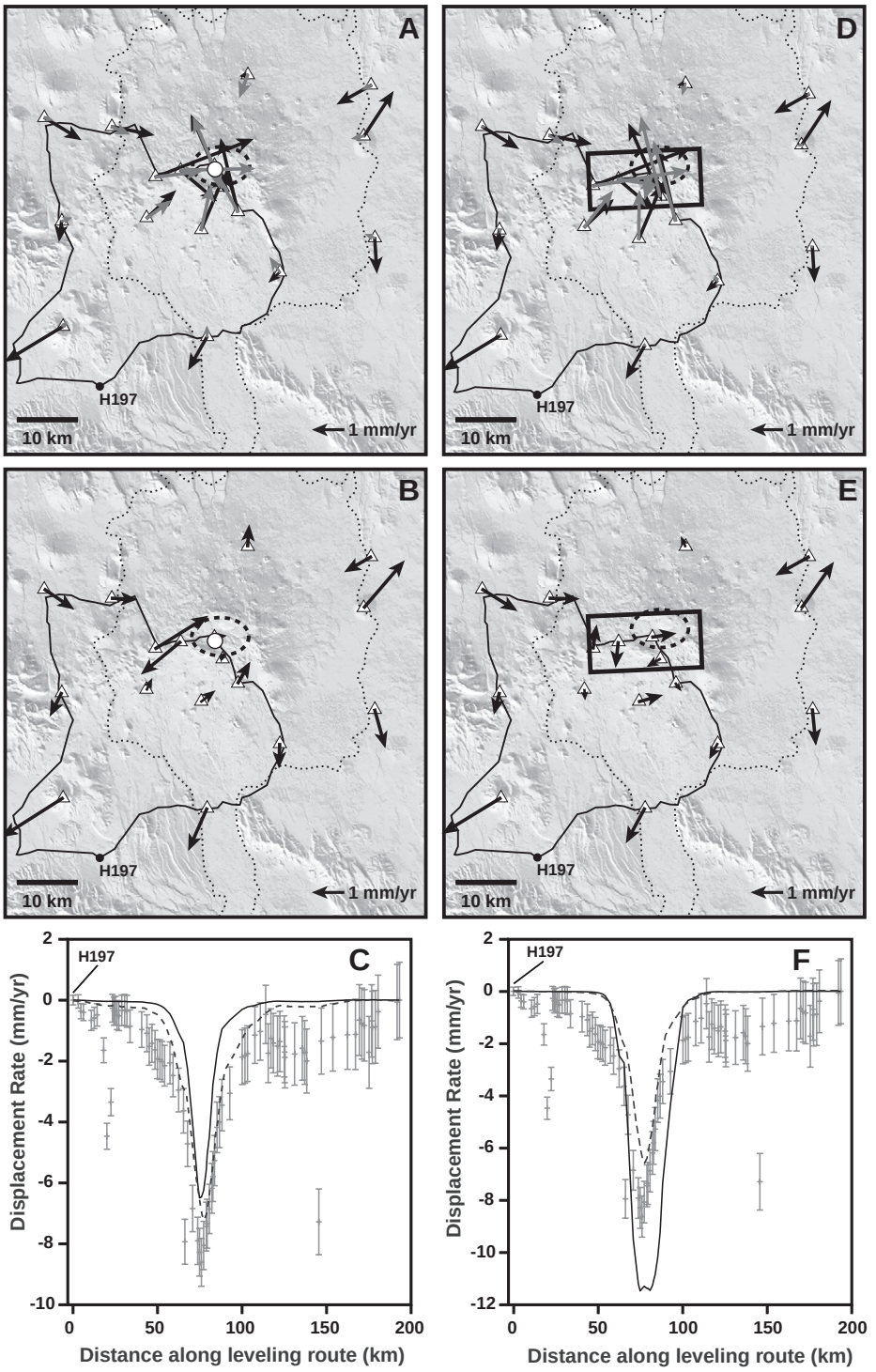
A
H197
10 km
1 mm/yr
D
H197
10 km
1 mm/yr
B
H197
10 km
1 mm/yr
E
H197
10 km
1 mm/yr
C
H197
Displacement Rate (mm/yr)
Distance along leveling route (km)
F
H197
Displacement Rate (mm/yr)
Distance along leveling route (km)

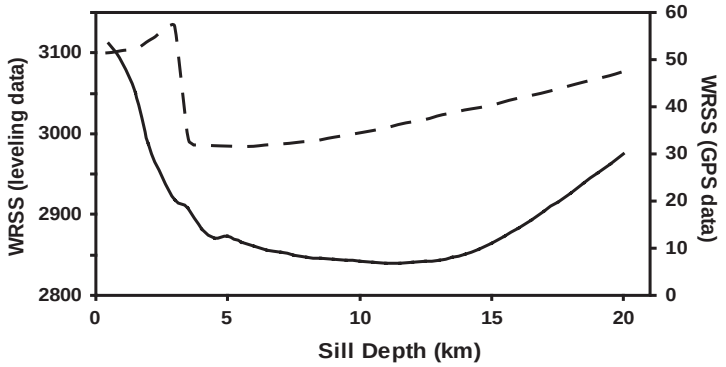


Fig. 7. Depth versus misfit (given as WRSS — Weighted Residual Sum of Squares) of best-fit closing horizontal dislocation (approximating a sill) from inversions of leveling (solid line) and GPS (dashed line) data at MLV. At each depth, all dislocation parameters (except depth, which is specified, and dip, which is constrained to be horizontal) are allowed to vary and the misfit of the best-fitting dislocation is plotted. Misfits are minimized at 11.5 and 5 km depths for leveling and GPS data, respectively. However, there is little variation in the leveling misfits for dislocations between approximately 5 and 15 km, and for GPS misfits between 4 and 10 km, suggesting that sill depths are not well constrained between these values in models based on either dataset.

tion in the center of the caldera than on the caldera rim. She hypothesizes that either a large basin already existed at the site of the present MLV caldera or the center of the caldera has subsided relative to its margins at a rate of 1.3 to 2.4 mm/yr (assuming subsidence began immediately after emplacement of the "dacite tuff of antelope well"). The rate would be even lower if caldera down-dropping had accompanied eruption of the tuff. The current subsidence rate of the caldera center relative to the rim is 4.9 mm/yr (Dzurisin et al., 1991, 2002), which is anomalously high when put into this geologic context. Thus, the current subsidence must be a relatively recent process at MLV.

In an attempt to constrain the mechanism of deformation at MLV, we examine the feasibility of several models that have been invoked to explain subsidence in other volcanic regions using a variety of methods. GPS and leveling data serve to test the hypotheses.

### 7.1. Volume loss at depth

Previous geodetic and modeling studies have found that magma removal from a shallow chamber (often due to emptying of a magma reservoir by eruption) is easily modeled by a point source of volume contraction (Mogi, 1958; Dvorak and Dzurisin, 1997). After the 1991 eruption of Hekla volcano in Iceland, horizontal displacements from GPS were radially towards the summit of the volcano (Sigmundsson et al., 1992). Sigmundsson et al. (1992) interpreted the signal as resulting from deflation of a subvolcanic magma chamber following the

Fig. 6. Model results from inversions of GPS data. In parts A, B, D, and E, solid line is the 1954–1989 leveling circuit of Dzurisin et al. (1991, 2002), dotted line marks the approximate aerial extent of MLV lava flows (Donnelly-Nolan, 1988), and dashed ellipse outlines MLV caldera. The location of leveling benchmark H197 is noted by a black circle and GPS sites are represented by white triangles. The white circle (in parts A and B) and black rectangular outline (in parts D and E) show the locations of the best fitting point and sill sources, respectively. Error ellipses on GPS velocities were omitted for clarity (see Fig. 4). A) Observed (black) and modeled (gray) horizontal displacements predicted by the best fitting point source of volume loss. B) Residual horizontal displacements after removal of point source model velocities. C) Comparison of leveling data (with 1-sigma error bars) to best fitting point source models from this study (solid line) and Dzurisin et al. (2002) (dashed line). Data are relative to benchmark H197, which is assumed to be stable, and distance is clockwise around the leveling circuit from that point. D) Observed (black) and modeled (gray) horizontal displacements predicted by the best fitting sill source. E) Residual horizontal displacements after removal of sill source model velocities. F) Comparison of leveling data (with 1-sigma error bars) to best fitting sill source models from this study (solid line) and Dzurisin et al. (2002) (dashed line). Data are displayed using the same convention as in part C, though note that the vertical scale is different.

eruption. Similar measurements and interpretations have been made in Hawaii (e.g., Delaney and McTigue, 1994; Johnson et al., 2000), Alaska (Lu et al., 2000a), and elsewhere around the world. Additionally, volcano deflation may be caused by lateral transport of magma in the subsurface away from the source region, which is common at Kilauea volcano in Hawaii (e.g., Delaney and McTigue, 1994; Cervelli et al., 2002), or by magma that drains from a shallow chamber to a deeper reservoir, as appears to be occurring at Askja volcano, Iceland, based on repeat microgravity measurements (De Zeeuw-van Dalfsen et al., 2005).

Volume loss due to eruption from a subsurface chamber is probably not a viable mechanism for subsidence at MLV. The most recent eruption occurred when about 1 $km^3$ of rhyolite and dacite were extruded at Glass Mountain at ~900 yr BP. It is unlikely that deflation is continuing due to the subsurface volume loss during that event. Drainage of magma from a crustal source to a deeper reservoir is a possibility considering that the range of modeled source depths (discussed above) includes the depth of a zone of potential melt at 4–6 km (Evans and Zucca, 1988; Chiarabba et al., 1995), and a long period earthquake 15 km beneath the caldera in 1989 suggests the presence of liquid magma at greater depths (Pitt et al., 2002). Microgravity measurements collected over time, which can detect changes in the mass distribution of the subsurface (Battaglia et al., 1999; De Zeeuw-van Dalfsen et al., 2005), are required to rigorously test this mechanism.

A non-magmatic mechanism of volume loss at depth is fluid withdrawal from a shallow hydrothermal system. Fournier (1989) attributed episodic subsidence of Yellowstone caldera to crystallization of rhyolitic magma and associated release of aqueous magmatic fluids. Although MLV does host a hydrothermal system (Lowenstern et al., 2003, and references therein), the steady rate of subsidence argues against such a source. Deformation thought to be related to hydrothermal activity at Yellowstone (Dzurisin et al., 1999) and the Coso Hot Springs in eastern California (Wicks et al., 2001) includes alternating cycles of subsidence and uplift over annual to decadal timescales from sources that can be approximated by deflating horizontal dislocations at shallow depths. The steady rate of subsidence since 1954 argues against a mechanism including fluid loss from a hydrothermal reservoir.

### 7.2. Cooling and crystallization of magma

Volume loss due to cooling of a magma body is a function of two processes: 1) crystallization of liquid melt, which partitions the volatiles into the remaining melt until saturation is reached, bubbles form, and are removed, and 2) thermal contraction of a cooling mass of sub-solidus crystalline rock (Fournier, 1989; Dzurisin et al., 2002). Several authors have suggested cooling and crystallization as a subsidence mechanism at recently active volcanoes. Radar interferometry results from Krafla volcano, Iceland, show subsidence that is modeled by volume loss from a point source at 3 km depth. The deflation rate is decreasing with time, suggesting thermal contraction of a magma reservoir that was probably the source of the 1975–1984 eruptive episode (Sigmundsson et al., 1997). Similarly, deflation of Askja volcano (also in Iceland), measured by leveling and GPS, has also been attributed to volume loss due to cooling and crystallization of magma (Sturkell and Sigmundsson, 2000).

Dzurisin et al. (2002) discuss the application of cooling and crystallization models to MLV and conclude that the current subsidence rate requires either an improbably large cooling volume (>>10 $km^3$) or an unrealistically rapid crystallization rate. In addition, the cooling process must produce a constant subsidence rate over a ~50 yr period to explain the results of repeated leveling surveys. However, they consider only the inferred ~10 $km^3$ partially molten body beneath the caldera as the source of cooling and crystallization. A larger and more realistic source of thermal contraction may be the column of hot intrusions and country rock that underlie the volcano (Fig. 2) (Donnelly-Nolan, 1988). This relatively Hot roughly Cylindrical Volume (HCV) received an input of heat approximately 13,000 yr BP when a major episode of mafic volcanism began. Migration of melt through the column of rock under MLV to the surface would have resulted in both the emplacement of molten intrusions and heating of surrounding country rock. The HCV would cool and contract following the magma migration event. To investigate the thermoelastic deformation of the HCV over a period of 10,000 yr, we included surface topography and known

subsurface structure in a linear elastic finite element model using the commercially available ABAQUS software. The model does not account for intrusive heat input that must have accompanied volcanic activity within the past 5000 yr. Late Holocene silicic lava flows contain mafic inclusions which suggest recent unerupted mafic inputs (Donnelly-Nolan et al., 1990), but the early post-glacial mafic eruptions comprise ~65% of the volume erupted during the Holocene suggesting that they represent the greatest heat input. The problem domain simulated by the axisymmetric model is 100 km wide and 50 km deep (to avoid edge effects), and the base and far radial edges are fixed (Fig. 8). The mechanical properties of the subsurface are based on the velocity model of Zucca et al. (1986), Poisson's ratios of Christensen (1996), and the conceptual model of Dzurisin et al. (1991). The HCV is modeled as extending from the mantle to a depth of 4 km under the volcano with an initial temperature of 800 °C (which is also the modeled

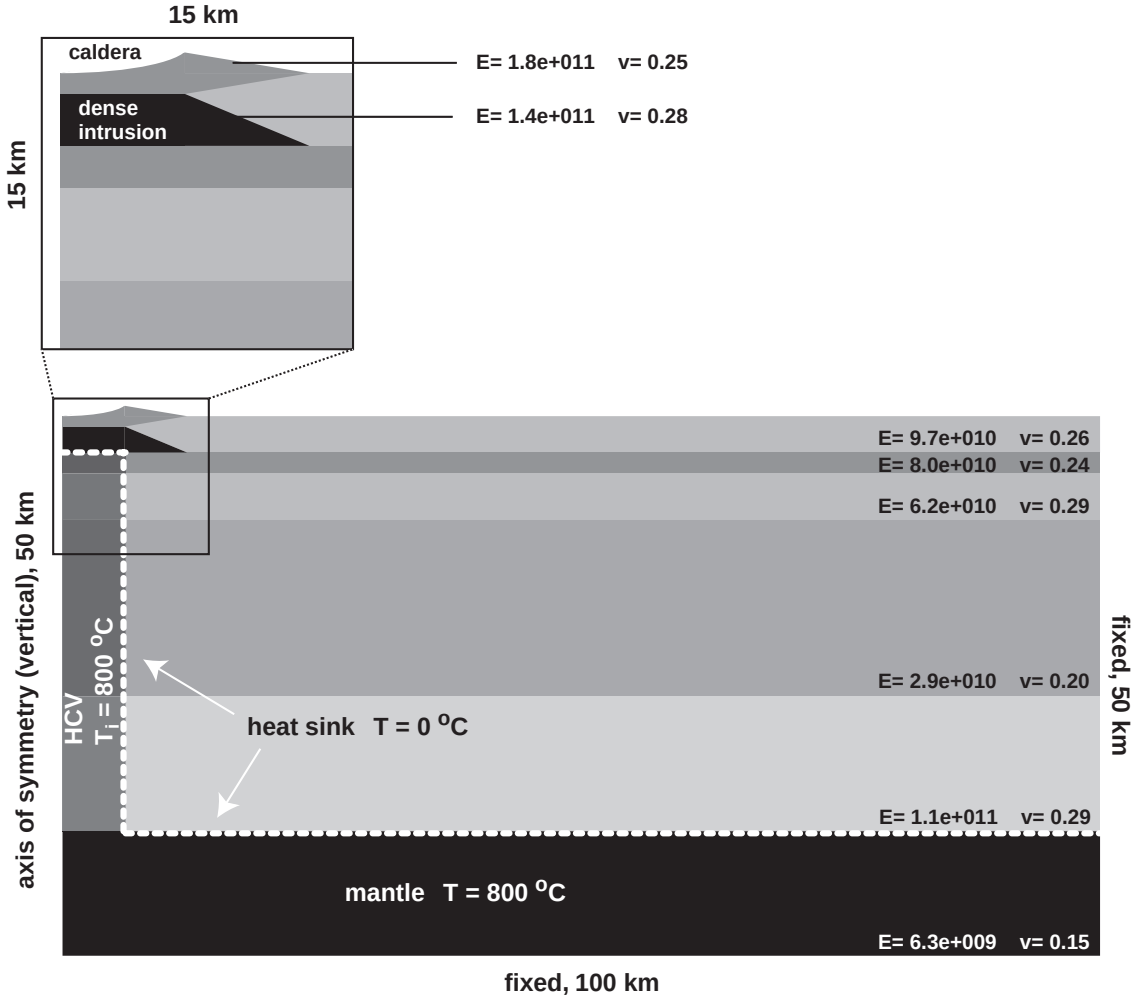


Fig. 8. Configuration for the finite element model. The problem domain is axisymmetric, and the base and distal radial boundaries are fixed. The upper extent of the model is a free surface. Material properties ($E$ = Young's modulus, $v$ = Poisson's ratio) are taken from Zucca et al. (1986) and Christensen (1996), and the geometry is based on the conceptual model of Dzurisin et al. (1991). The model includes a dense intrusive complex below the topographic expression of MLV. The initial temperature of the Hot, roughly Cylindrical Volume (HCV — to the left and below the white dashed line) is 800 °C, and country rock acts as a heat sink at 0 °C.

temperature of the base of the crust in the MLV region as predicted by subduction zone geotherms of Turcotte and Schubert (1982, p. 196)). The surrounding country rock, at 0 °C, serves as a heat sink. This configuration is reasonable if the groundwater flow system transports heat relatively efficiently, with respect to heat transport limited to thermal conduction through a dry rock system. A comparison of the hydraulic (Saar and Manga, 2004) and thermal diffusivities suggests this is likely to be the case. The modeled annual subsidence after 10,000 yr is a good fit to the vertical displacement rate and geometry determined from leveling when increased by a factor of 7 (Fig. 9A). Deviations from the simple geometric configuration of the hot cylinder, additional volumetric decreases due to crystallization of the feeder complex within the hot cylinder, a higher initial temperature than 800 °C, a locally overestimated rigidity,

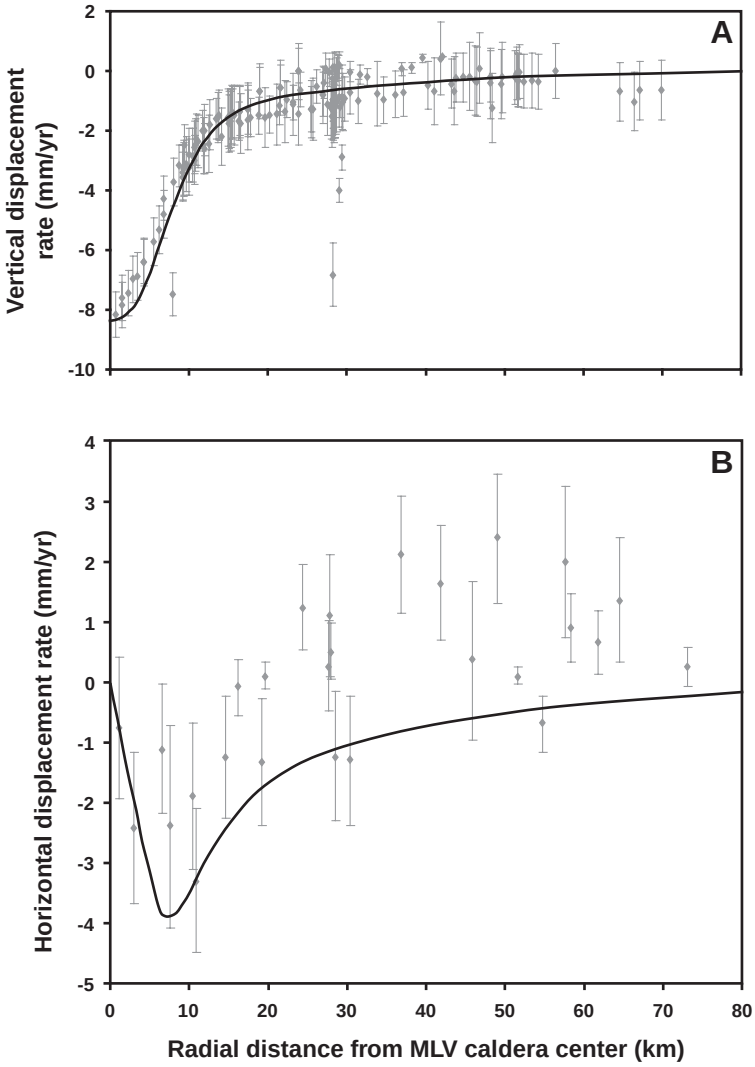


Fig. 9. Predicted deformation of thermoelastic finite element model (black line) when increased by a factor of 7. (A) Vertical displacements predicted by the model with radial distance from the center of subsidence. Gray diamonds with error bars are leveling results. (B) Horizontal displacements predicted by the model (negative is towards MLV caldera) with radial distance from the center of subsidence. Gray diamonds with error bars show the radial component of horizontal deformation from GPS.

and input of additional heat through intrusive activity over time are some of the factors that may account for the prediction errors. Thus, the model represents a lower limit to the magnitude of expected deformation. Note that the ratio of horizontal to vertical predicted displacements is larger than that measured by GPS and leveling (Fig. 9B). This proportionality should remain constant regardless of variations in model parameters, leading us to conclude that thermoelastic contraction of the HCV does not fully explain the present deformation.

### 7.3. Surface loading

MLV is the largest volcano by volume in the Cascade volcanic arc (Donnelly-Nolan, 1988; Dzurisin et al., 1991), and subsidence will undoubtedly occur due to loading by the edifice and subvolcanic intrusions. Surface loading is a significant deformation mechanism at large basaltic shields, especially ocean islands, extraterrestrial volcanoes, and seamounts (e.g. Walcott, 1970; Watts et al., 1975; Lambeck and Nakiboglu, 1980; Williams and Zuber, 1995; McGovern et al., 1999).

Brotchie and Silvester (1969) and Brotchie (1971) present an axisymmetric solution for a load on the surface of a spherical, liquid filled shell. The thickness of the shell is the brittle upper crust, while the radius of the sphere corresponds to the planetary radius. At MLV we assume the shell thickness is 10 km to approximate the depth to the brittle–ductile transition, though that rheological boundary can be as shallow as 3 km in volcanic regions, (e.g., Reches and Fink, 1988). Gravity evidence indicates a bulk density of approximately 2400 kg/m$^3$ in the MLV region (Finn and Williams, 1982). A simple point source load equivalent to the mass of the volcano predicts a much broader pattern of subsidence than is observed by leveling ("thin shell" in Fig. 10). A more realistic approximation of MLV topography using a series of stacked concentric cylinders (Comer et al., 1985) narrows the subsiding area's radius ("stacked cylinders" in Fig. 10) but still does not approximate the pattern of subsidence. Increasing the shell thickness to approximate that of the entire lithosphere (100 km) only serves to increase the area over which subsidence occurs ("thick shell" in Fig. 10). Fitting the pattern of the measured vertical displacements can be

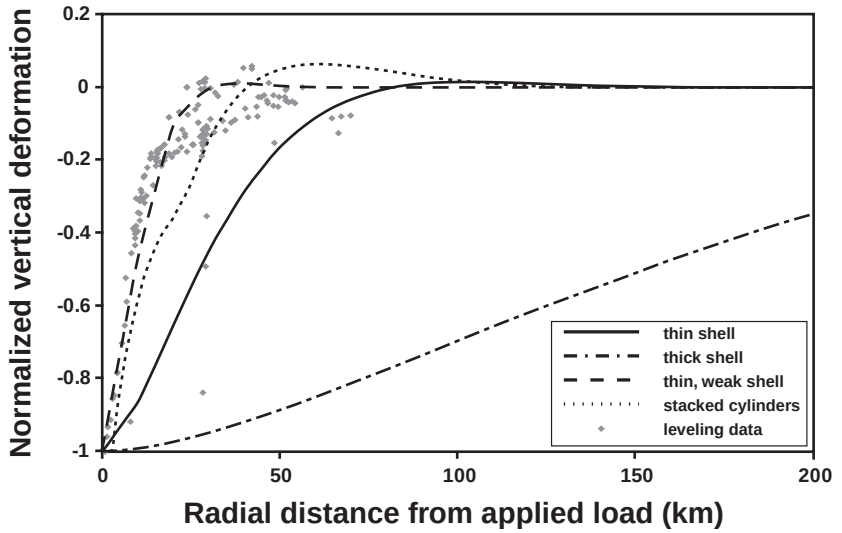


Fig. 10. Elastic models of vertical deformation due to crustal loading at MLV with radial distance from the applied load. Leveling results are gray diamonds (error bars omitted for clarity — see Fig. 9A). Displacements are normalized so that the maximum vertical deformation (in both models and leveling data) is equal to −1 (to facilitate comparison of observed and predicted subsidence patterns). The "thin shell" and "stacked cylinders" models include a shell thickness of 10 km (the same order as the brittle crust) and a Young's modulus of $7 \times 10^{10}$ Pa. The "thick shell" model has the same Young's modulus but a shell thickness of 100 km (approximating the lithosphere). A shell thickness of 10 km and a Young's modulus of $1 \times 10^9$ Pa are used in the "thin, weak shell" model.

accomplished using a point source loading a 10 km-thick shell with a Young's modulus an order of magnitude lower than inferred for normal crust ($1 \times 10^9$ Pa, the "thin, weak shell" in Fig. 10, versus $7 \times 10^{10}$ Pa, which was used for all other models). Geological evidence suggests thermally weakened crust in the MLV region (Dzurisin et al., 1991; Blakely et al., 1997), and the lower Young's modulus is similar to that found by workers at other volcanoes (Rubin and Pollard, 1987; Schultz, 1993). Thus some combination of load geometry, thin brittle upper crust, and Young's modulus may be used to fit the observed subsidence pattern. However, these elastic models do not provide information about the predicted subsidence rate. The Island of Hawaii is many times larger than MLV and up to 4.8 mm/yr has been attributed to surface loading there (Moore, 1971). The rate should be proportionally smaller at MLV, much less than that which has been observed since 1954. Further, all models of crustal flexure predict an annulus of uplift at some distance from the load. Preliminary results from a leveling line that was surveyed in 1940 and 2003 and extends 120 km east of MLV do not indicate any deformation that might be related to flexural uplift, though the signal may be too small to be measurable.

### 7.4. Crustal extension

Extensional tectonism is almost certainly occurring around MLV based on both recent faulting events and the presence of numerous normal faults in the region (Blakely et al., 1997). Following Novak and Bacon (1986), Donnelly-Nolan (written communication, 2004) speculates that the abundance of rhyolitic volcanism in the last ~2000 yr may reflect a high extension rate relative to other time periods, which would encourage rising basalts to fill opening spaces in the crust and promote the generation of more silicic magmas. A relatively high rate of tectonic extension could explain the anomalous subsidence rate, but is not consistent with GPS results which show no resolvable extensional strain across the region (Figs. 3 and 4). Blakely et al. (1997) demonstrated that MLV is located at a change in the geometry of regional faulting, which may facilitate volcanism and subsidence. Focal mechanisms from the area of MLV caldera during the 1988–89 earthquake swarm are diverse (Fig. 1C), consistent with the faulting pattern (Weaver and Hill, 1979). However, the high rate of current subsidence cannot realistically extend into the past more than several thousand years; therefore, the tectonic subsidence mechanism requires a recent change in the tectonics of the region, which is unlikely. Extension and shear are actively occurring in the MLV region and will probably enhance any existing subsidence mechanisms, but cannot account for the overall deformation pattern observed since 1954.

## 8. Conclusions and future work

Any explanation of subsidence at MLV must account for five factors: 1) the anomalously high rate of present subsidence relative to the overall history of the volcano, 2) the broad subsidence pattern with comparatively smaller horizontal displacements near the summit of MLV, 3) the spatial and temporal stability of the subsidence since 1954, 4) the apparent lack of significant mass or thermal input in the past ~900 yr, and 5) the subsurface structure inferred from geophysical investigations. Based on the preceding discussion, it is clear that no single mechanism can satisfy all five constraints, but many of the mechanisms meet some of the requirements. As a result, we favor a combination of factors as the cause of subsidence at MLV. Surface loading and tectonic extension (with shear) are almost certainly acting on the volcano, but cannot explain the high present vertical displacements relative to geologic rates. Likewise, thermoelastic contraction of a hot cylindrical volume of rock beneath MLV following a magma migration event at the end of the most recent glaciation is an attractive hypothesis but predicts a horizontal displacement pattern greater than that measured by GPS. Dzurisin et al. (1991, 2002) suggested that surface loading combined with extension of a hot weak crust are the dominant causes of subsidence. This mechanism, combined with cooling of hot rock beneath the volcano, remains the most likely explanation for the deformation because it incorporates processes that are known to be occurring. The anomalously high present subsidence rate may be caused by recent heating of the subsurface during the mafic magmatic episode that occurred about ~13,000 yr ago. The input of heat would further weaken the subsurface, and subsequent

cooling of the affected mass would result in volume contraction that may still be occurring today.

Withdrawal of either magma or hydrothermal fluids (to the surface or deeper levels) as a cause for subsidence of MLV is not favored, which has significant implications for the interpretation of geodetic data at other volcanic centers. Simple elastic models of volume change at depth are commonly used to explain surface displacements at volcanoes. As shown by Dzurisin et al. (2002), point and sill sources in an elastic half space fit vertical displacements at MLV well and suggest the possibility that fluids are moving in the subsurface. However, measurements of horizontal motion with GPS are not consistent with such models. Indeed, it may not be appropriate to apply these simple models of volume change to MLV deformation. The same is probably true at other volcanoes, and it is important that analyses of volcano deformation consider mechanisms beyond volume change in subsurface fluid reservoirs.

Future work planned at MLV will provide tighter constraints on the mechanism of deformation. Measurements of microgravity over time coupled with surface displacements will detect mass changes at depth (Battaglia et al., 1999; De Zeeuw-van Dalfsen et al., 2005), and would help to test our assertion that fluid migration is not occurring at MLV. In addition, the Mt. Shasta/MLV area is the site of a Plate Boundary Observatory volcano cluster and is planned to be instrumented with ~20 continuous GPS stations by the year 2010. The network should provide better resolution of both horizontal and vertical displacement patterns, which will be valuable for testing models of volcano deformation presented here and elsewhere.

## Acknowledgements

This work was completed as part of Poland's doctoral dissertation at Arizona State University, which was supported by a National Defense Science and Engineering Graduate Fellowship. The authors wish to thank the 1996, 1999, 2000, 2003, and 2004 GPS crews for their hard work: Miya Barr, Andre Bassett, James Burke, Branden Christensen, Shelley Crouse, Elliot Endo, Sarah Fein, Kathryn Flynn, Ben Gregory, Chris Harpel, Bridget Hellwig, Jason Hughes, Heidi Iverson, Stephanie Konfal, Peter Krag, Sally Lamb, Jeff Light, William Loskutoff, Rich Loverne, Chantelle Lucas, Aaron Lyman, Henry Miyashita, Kurt Parker, Barbara Poland, Jim Poland, Steve Schilling, Paul Schultz, James Tautfest, Sean Taylor, Sarah Thompson, David Wieprecht, Lily Wong, and Chimi Yi. The cooperation of Lava Beds National Monument and the Modoc, Shasta, and Klamath National Forests is greatly appreciated. Figs. 1 and 3–6 were created using the Generic Mapping Tools (GMT) software (Wessel and Smith, 1998). Bill Hammond shared GPS data from the MLV region, which was essential for defining the rigid block rotation. ERS-1/2 data was supplied by the European Space Agency under an AO3 grant. Julie Donnelly-Nolan and Jake Lowenstern shared their knowledge of the geology of MLV, which helped guide our interpretations. Bill Chadwick, Tim Dixon, Andrew Newman, Jake Lowenstern, and Julie Donnelly-Nolan provided helpful reviews. This research was supported by grants from the Northern California Geological Survey, Sigma Xi Scientific Research Society, USGS Jack Kleinman Internship for Volcano Research, UC Davis President's Undergraduate Fellowship Program, and NASA Solid Earth and Natural Hazards Grant NAG 57573.

## References

Anderson, C.A., 1941. Volcanoes of the Medicine Lake highland, California. University of California Publications in Geological Sciences 25, 347–422.

Argus, D.F., Gordon, R., 1991. Pacific–North American plate motion from very long baseline interferometry compared with motion inferred from magnetic anomalies, transform faults, and earthquake slip vectors. Journal of Geophysical Research 95, 17315–17324.

Battaglia, M., Roberts, C., Segall, P., 1999. Magma intrusion beneath Long Valley Caldera confirmed by temporal changes in gravity. Science 285, 2119–2122.

Bennett, J.H., Sherburne, R.W., Cramer, C.H., Chesterman, C.W., Chapman, R.H., 1979. Stephens Pass earthquakes, Mount Shasta — August 1978, Siskiyou County, CA. California Geology 32, 27–34.

Bennett, R.A., Wernicke, B.P., Niemi, N.A., Friedrich, A.M., Davis, J.L., 2003. Contemporary strain rates in the northern Basin and Range province from GPS data. Tectonics 22, doi:10.1029/2001TC001355.

Blakely, R.J., Christiansen, R.L., Guffanti, M., Wells, R.E., Donnelly-Nolan, J.M., Muffler, L.J.P., Clynne, M.A., Smith, J.G., 1997. Gravity anomalies, Quaternary vents, and Quaternary faults in the southern Cascade Range, Oregon and California;

implications for arc and backarc evolution. Journal of Geophysical Research 102, 22513–22527.
Brotchie, J.F., 1971. Flexure of a liquid-filled spherical shell in a radial gravity field. Modern Geology 3, 15–23.
Brotchie, J.F., Silvester, R., 1969. On crustal flexure. Journal of Geophysical Research 74, 5240–5252.
Cervelli, P., Segall, P., Amelung, F., Owen, H., Miklius, S., Lisowski, A., 2002. The 12 September 1999 Upper East Rift Zone dike intrusion at Kilauea Volcano, Hawaii. Journal of Geophysical Research 107, doi:10.1029/2001JB000602.
Chiarabba, C., Amato, A., Evans, J.R., 1995. Variations on the NeHT high-resolution tomography method: a test of technique and results for Medicine Lake Volcano, northern California. Journal of Geophysical Research 100, 4035–4052.
Christensen, N.I., 1996. Poisson's ratio and crustal seismology. Journal of Geophysical Research 101, 3139–3156.
Comer, R.P., Solomon, S.C., Head, J.W., 1985. Thickness of the lithosphere from the tectonic response to volcanic loads. Reviews of Geophysics 23, 61–92.
Delaney, P.T., McTigue, D.F., 1994. Volume of magma accumulation or withdrawal estimated from surface uplift or subsidence, with application to the 1960 collapse of Kilauea Volcano. Bulletin of Volcanology 56, 417–424.
de Zeeuw-van Dalfsen, E., Rymer, H., Sigmundsson, F., Sturkell, E., 2005. Net gravity decrease at Askja volcano, Iceland: constraints on processes responsible for continuous caldera deflation, 1988–2003. Journal of Volcanology and Geothermal Research 139, 227–239.
Dixon, T.H., Robaudo, S., Lee, J., Reheis, M.C., 1995. Constraints on present-day Basin and Range deformation from Space Geodesy. Tectonics 14, 755–772.
Dixon, T.H., Miller, M., Farina, F., Wang, H., Johnson, D., 2000. Present-day motions of the Sierra Nevada block and some tectonic implications for the Basin and Range province, North American Cordillera. Tectonics 19, 1–24.
Dokka, R.K., Travis, C.J., 1990a. Late Cenozoic strike-slip faulting in the Mojave Desert, California. Tectonics 9, 311–340.
Dokka, R.K., Travis, C.J., 1990b. Role of the eastern California shear zone in accommodating Pacific–North American plate motion. Geophysical Research Letters 17, 1323–1326.
Donnelly-Nolan, J.M., 1988. A magmatic model of Medicine Lake Volcano, California. Journal of Geophysical Research 93, 4412–4420.
Donnelly-Nolan, J.M., Nolan, K.M., 1986. Catastrophic flooding and eruption of ash-flow tuff at Medicine Lake Volcano, California. Geology 14, 875–878.
Donnelly-Nolan, J.M., Ramsey, D.W., 2001. Geologic mapping of Medicine Lake Volcano, CA, USA. EOS, Transactions of the American Geophysical Union 82 (Abstract V22B-1043).
Donnelly-Nolan, J.M., Champion, D.E., Miller, C.D., Grove, T.L., Trimble, D.A., 1990. Post-11,000-year volcanism at Medicine Lake Volcano, Cascade Range, Northern California. Journal of Geophysical Research 95, 19693–19704.
Donnelly-Nolan, J.M., Champion, D.E., Grove, T.L., Baker, M.B., Taggart Jr., J.E., Bruggman, P.E., 1991. The giant crater lava field; geology and geochemistry of a compositionally zoned, high-alumina basalt to basaltic andesite eruption at Medicine Lake Volcano, California. Journal of Geophysical Research 96, 21843–21863.
Dvorak, J.J., Dzurisin, D., 1997. Volcano geodesy; the search for magma reservoirs and the formation of eruptive vents. Reviews of Geophysics 35, 343–384.
Dzurisin, D., Donnelly-Nolan, J.M., Evans, J.R., Walter, S.R., 1991. Crustal subsidence, seismicity, and structure near Medicine Lake Volcano, California. Journal of Geophysical Research 96, 16319–16333.
Dzurisin, D., Poland, M.P., Bürgmann, R., 2002. Steady subsidence of Medicine Lake Volcano, Northern California, revealed by repeated leveling surveys. Journal of Geophysical Research 107, 2372, doi:10.1029/2001JB000893.
Dzurisin, D., Wicks Jr., C., Thatcher, W., 1999. Renewed uplift at the Yellowstone Caldera measured by leveling surveys and satellite radar interferometry. Bulletin of Volcanology 61, 349–355.
Eichelberger, J.C., 1981. Mechanism of magma mixing at Glass Mountain, Medicine Lake Highland volcano, California. In: Johnston, D.A., Donnelly-Nolan, J.M. (Eds.), Guides to Some Volcanic Terranes in Washington, Idaho, Oregon, and Northern California, U.S. Geological Survey Circular, vol. 838, pp. 183–189.
Evans, J.R., Zucca, J.J., 1988. Active high-resolution seismic tomography of compressional wave velocity and attenuation structure at Medicine Lake Volcano, Northern California cascade range. Journal of Geophysical Research 93, 15016–15036.
Fink, J.H., Pollard, D.D., 1983. Structural evidence for dikes beneath silicic domes, Medicine Lake Highland Volcano, California. Geology 11, 458–461.
Finn, C., Williams, D.L., 1982. Gravity evidence for a shallow intrusion under Medicine Lake Volcano, California. Geology 10, 503–507.
Fournier, R.O., 1989. Geochemistry and dynamics of the Yellowstone National Park hydrothermal system. Annual Review of Earth and Planetary Sciences 17, 13–53.
Fuis, G.S., Zucca, J.J., Mooney, W.D., Milkereit, B., 1987. A geologic interpretation of seismic refraction results in northeastern California. Geological Society of America Bulletin 98, 53–65.
Gerlach, D.C., Grove, T.L., 1982. Petrology of Medicine Lake highland volcanics: characterization of endmembers of magma mixing. Contributions to Mineralogy and Petrology 80, 147–159.
Grove, T.L., Donelly, N.J.M., 1986. The evolution of young silicic lavas at Medicine Lake Volcano, California; implications for the origin of compositional gaps in calc-alkaline series lavas. Contributions to Mineralogy and Petrology 92, 281–302.
Grove, T.L., Gerlach, D.C., Sando, T.W., 1982. Origin of calc-alkaline series lavas at Medicine Lake Volcano by fractionation, assimilation and mixing. Contributions to Mineralogy and Petrology 80, 160–182.
Grove, T.L., Kinzler, R.J., Baker, M.B., Donnelly, N.J.M., Lesher, C.E., 1988. Assimilation of granite by basaltic magma at burnt lava flow, Medicine Lake Volcano, Northern California; decoupling of heat and mass transfer. Contributions to Mineralogy and Petrology 99, 320–343.

Hammond, W.C., Thatcher, W., 2003. Crustal Deformation of the Northern Basin and Range from Measurement with the Global Positioning System. EOS, Transactions, American Geophysical Union 84, Fall Meeting Supplement. Abstract G32B-07.

Hammond, W.C., Thatcher, W., 2004. Contemporary tectonic deformation of the Basin and Range province, western United States: 10 years of observation with the Global Positioning System. Journal of Geophysical Research 109, doi:10.1029/2003JB002746.

Heiken, G., 1978. Plinian-type eruptions in the Medicine Lake Highland, California, and the nature of the underlying magma. Journal of Volcanology and Geothermal Research 4, 375–402.

Hoffmann, J., Zebker, H.A., 2003. Prospecting for horizontal surface displacements in Antelope Valley California, using satellite radar interferometry. Journal of Geophysical Research 108, 6011, doi:10.1029/2003JF000055.

Jennings C.W., 1994. Fault activity map of California and adjacent areas with locations and ages of recent volcanic eruptions. California Division of Mines and Geology Geologic Data Map No. 6, 1:750,000.

Johnson, D.J., Sigmundsson, F., Delaney, P.T., 2000. Comment on "Volume of magma accumulation or withdrawal estimated from surface uplift or subsidence with application to the 1960 collapse of Kilauea volcano" by P.T. Delaney and D. F. McTigue. Bulletin of Volcanology 61, 491–493.

Lambeck, K., Nakiboglu, S.M., 1980. Seamount loading and stress in the ocean lithosphere. Journal of Geophysical Research 85, 6403–6418.

Lewis, J.C., Unruh, J.R., Twiss, R.J., 2003. Seismogenic strain and motion of the Oregon coast block. Geology 31, 183–186.

Lowenstern, J.B., 1999. Late Quaternary U–Pb and Ar–Ar ages of granitic intrusions beneath Medicine Lake volcano, California, USA. EOS, Transactions of the American Geophysical Union 80, 1130–1131.

Lowenstern, J.B., Persing, H.M., Wooden, J.L., Lanphere, M., Donnelly-Nolan, J.M., Grove, T.L., 2000. U–Th dating of single zircons from young granitoid xenoliths: new tools for understanding volcanic processes. Earth and Planetary Science Letters 183, 291–302.

Lowenstern, J.B., Donnelly-Nolan, J., Wooden, J.L., Charlier, B.L.A., 2003. Volcanism, Plutonism, and Hydrothermal Alteration at Medicine Lake volcano, California, Twenty-Eighth Workshop on Geothermal Reservoir Engineering, Stanford University, California, pp. 1–8.

Lu, Z., Mann, D., Freymueller, J.T., Meyer, D.J., 2000. Synthetic aperture radar interferometry of Okmok volcano, Alaska: radar observations. Journal of Geophysical Research 105, 10791–10806.

Lu, Z., Wicks, C., Dzurisin, D., Thatcher, W., Freymueller, J.T., McNutt, S.R., Mann, D., 2000. Aseismic inflation of Westdahl volcano, Alaska, revealed by satellite radar interferometry. Geophysical Research Letters 27, 1567–1570.

McCaffrey, R., Long, M.D., Goldfinger, C., Zwick, P.C., Nabelek, J.L., Johnson, C.K., Smith, C., 2000. Rotation and plate locking at the southern Cascadia subduction zone. Geophysical Research Letters 27, 3117–3120.

McGovern, P.J., Solomon, S.C., Faulkner, S.E., Head, J.W., Smith, D.E., Zuber, M.T., 1999. Extension and Volcanic Loading at Alba Patera: Insights from MOLA Observations and Loading Models, Lunar and Planetary Science Conference 30. Abstract 1697.

Miller, M.M., Johnson, D.J., Dixon, T.H., Dokka, R.K., 2001a. Refined kinematics of the Eastern California Shear Zone from GPS observations, 1993–1998. Journal of Geophysical Research 106, 2245–2263.

Miller, M.M., Johnson, D.J., Rubin, C.M., Dragert, H., Wang, K., Qamar, A., Goldfinger, C., 2001b. GPS-determination of along-strike variation in Cascadia margin kinematics: implications for relative plate motion, subduction zone coupling, and permanent deformation. Tectonics 20, 161–176.

Mogi, K., 1958. Relations between the eruptions of various volcanoes and the deformations of the ground surfaces around them. Bulletin of the Earthquake Research Institute 36, 99–134.

Moore, J.G., 1971. Relationship between subsidence and volcanic load, Hawaii. Bulletin of Volcanology 34, 562–576.

Murray, M.H., Lisowski, M., 2000. Strain accumulation along the Cascadia subduction zone. Geophysical Research Letters 27, 3631–3634.

Novak, S.W., Bacon, C.R., 1986. Pliocene Volcanic Rocks of the Coso Range, Inyo County, California, US Geological Survey Professional Paper, vol. 1383. 44 pp.

Okada, Y., 1985. Surface deformation due to shear and tensile faults in a half-space. Bulletin of the Seismological Society of America 75, 1135–1154.

Page, W.D., Sawyer, T.L., McLaren, M.K., Savage, W.U., Wakabayashi, J., 1993. The Quaternary Tahoe–Medicine Lake Trough: the western margin of the Basin and Range transition, NW California. Abstracts with Programs — Geological Society of America 25, 131.

Patton, H.J., Zandt, G., 1991. Seismic moment tensors of western U.S. earthquakes and implications for the tectonic stress field. Journal of Geophysical Research 96, 18245–18259.

Peacock, M.A., 1931. The Modoc lava field, northern California. Geographical Review 21, 259–275.

Pease, R.W., 1969. Normal faulting and lateral shear in northeastern California. Geological Society of America Bulletin 80, 715–720.

Pezzopane, S.K., Weldon II, R.J., 1993. Tectonic role of active faulting in central Oregon. Tectonics 12, 1140–1169.

Pitt, A.M., Hill, D.P., Walker, S.W., Johnson, M.J.S., 2002. Mid-crustal, long-period earthquakes beneath northern California volcanic areas. Seismological Research Letters 73, 144–152.

Powers, H.A., 1932. The lavas of the Modoc Lava-Bed quadrangle, California. The American Mineralogist 17, 253–294.

Reches, Z., Fink, J., 1988. The mechanism of intrusion of the Inyo Dike, Long Valley Caldera, California. Journal of Geophysical Research 93, 4321–4334.

Ritter, J.R.R., Evans, J.R., 1997. Deep structure of Medicine Lake volcano, California. Tectonophysics 275, 221–241.

Roberts, C.T., 1984. Cenozoic evolution of the northwestern Honey Lake Basin, Lassen County, California. Colorado School of Mines Quarterly 80, 1–64.

Rubin, A.M., Pollard, D.D., 1987. Origins of blade-like dikes in volcanic rift zones. In: Decker, R.W., Wright, T.L., Stauffer, P.H. (Eds.), Volcanism in Hawaii, USGS Professional Paper, vol. 1350, pp. 1449–1470.

Saar, M.O., Manga, M., 2004. Depth dependence of permeability in the Oregon Cascades inferred from hydrogeologic, thermal, seismic, and magmatic modeling constraints. Journal of Geophysical Research 109, doi:10.1029/2003JB002855.

Sauber, J., Thatcher, W., Solomon, S.C., Lisowski, M., 1994. Geodetic slip rate for the eastern California shear zone and the recurrence time of Mojave desert earthquakes. Nature 367, 264–266.

Savage, J.C., Gan, W., Svarc, J.L., 2001. Strain accumulation and rotation in the Eastern California Shear Zone. Journal of Geophysical Research 106, 21995–22007.

Savage, J.C., Svarc, J.L., Prescott, W.H., Murray, M.H., 2000. Deformation across the forearc of the Cascadia subduction zone at Cape Blanco, Oregon. Journal of Geophysical Research 105, 3095–3102.

Schultz, R.A., 1993. Brittle strength of basaltic rock masses with applications to Venus. Journal of Geophysical Research 98, 10883–10895.

Sigmundsson, F., Einarsson, P., Bilham, R., 1992. Magma chamber deflation recorded by the global positioning system: the Hekla 1991 eruption. Geophysical Research Letters 19, 1483–1486.

Sigmundsson, F., Vadon, H., Massonnet, D., 1997. Readjustment of the Krafla spreading segment to crustal rifting measured by satellite radar interferometry. Geophysical Research Letters 24, 1843–1846.

Stanley, W.D., Mooney, W.D., Fuis, G.S., 1990. Deep crustal structure of the Cascade Range and surrounding regions from seismic refraction and magnetotelluric data. Journal of Geophysical Research 95, 19419–19438.

Sturkell, E., Sigmundsson, F., 2000. Continuous deflation of the Askja caldera, Iceland, during the 1983–1998 noneruptive period. Journal of Geophysical Research 105, 25671–25684.

Szeliga, W., Melbourne, T.I., Miller, M.M., Santillan, V.M., 2004. Southern Cascade episodic slow earthquakes. Geophysical Research Letters 31, doi:10.1029/2004GL020824.

Thatcher, W., Foulger, G.R., Julian, B.R., Svarc, J., Quilty, E., Bawden, G.W., 1999. Present-day deformation across the Basin and Range province, western United States. Science 283, 1714–1718.

Turcotte, D.L., Schubert, G., 1982. Geodynamics: Applications of Continuum Physics to Geological Problems. John Wiley and Sons, New York. 450 pp.

Walcott, R.I., 1970. Flexure of the lithosphere at Hawaii. Tectonophysics 9, 435–446.

Walter, S., Dzurisin, D., 1989. The September, 1988 earthquake swarm at Medicine Lake volcano, northern California. EOS, Transactions, American Geophysical Union 70 (43), 1189–1190.

Watts, A.B., Cochran, J.R., Selzer, G., 1975. Gravity anomalies and flexure of the lithosphere: a three-dimensional study of the Great Meteor Seamount, Northeast Atlantic. Journal of Geophysical Research 80, 1391–1398.

Weaver, C.S., Hill, D.P., 1979. Earthquake swarms and local crustal spreading along major strike-slip faults in California. Pure and Applied Geophysics 117, 51–64.

Wells, R.E., Simpson, R.W., 2001. Northward migration of the Cascadia forearc in the northwestern U.S. and implications for subduction deformation. Earth, Planets, and Space 53, 275–283.

Wells, R.E., Weaver, C.S., Blakely, R.J., 1998. Fore-arc migration in Cascadia and its neotectonic significance. Geology 26, 759–762.

Wessel, P., Smith, W.H.F., 1998. New, improved version of generic mapping tools released. EOS, Transactions of the American Geophysical Union 79, 579.

Wicks Jr., C.W., Thatcher, W., Monastero, F.C., Hasting, M.A., 2001. Steady state deformation of the Coso Range, east central California, inferred from satellite radar interferometry. Journal of Geophysical Research 106, 13769–13780.

Williams, K.K., Zuber, M.T., 1995. An experimental study of incremental surface loading of an elastic plate: application to volcano tectonics. Geophysical Research Letters 22, 1981–1984.

Wright, L., 1976. Late Cenozoic fault patterns and stress fields in the Great Basin and westward displacement of the Sierra Nevada block. Geology 4, 489–494.

Yamashita, K.M., Wieprecht, D.E., 1995. Bench mark descriptions and photographs for Global Positioning System (GPS) stations in the vicinity of Mt. Shasta and Medicine Lake, California, U. S. Geological Survey Open File Report 95-0811. 18 pp.

Yokoyama, I., 1971. Pozzuoli event in 1970. Nature 229, 532–533.

Zucca, J.J., Fuis, G.S., Milkereit, B., Mooney, W.D., Catchings, R.D., 1986. Crustal structure of northeastern California. Journal of Geophysical Research 91, 7359–7382.

Zumberge, J.F., Heflin, M.B., Jefferson, D.C., Watkins, M.M., Webb, F.H., 1997. Precise point positioning for the efficient and robust analysis of GPS data from large networks. Journal of Geophysical Research 102, 5005–5017.